TRANSPARENT
PROCESS

EMBO
reports

The tumour suppressor OPCML promotes AXL inactivation by the phosphatase PTPRG in ovarian cancer

Jane Antony[1,2,3,†] (iD), Elisa Zanini[1] (iD), Zoe Kelly[1], Tuan Zea Tan[2] (iD), Evdoxia Karali[1], Mohammad Alomary[1], Youngrock Jung[1], Katherine Nixon[1], Paula Cunnea[1], Christina Fotopoulou[1], Andrew Paterson[1], Sushmita Roy-Nawathe[1], Gordon B Mills[4], Ruby Yun-Ju Huang[2,5], Jean Paul Thiery[2,6,7] (iD), Hani Gabra[1,8,*] (iD) & Chiara Recchi[1,**] (iD)

Abstract

In ovarian cancer, the prometastatic RTK AXL promotes motility, invasion and poor prognosis. Here, we show that reduced survival caused by AXL overexpression can be mitigated by the expression of the GPI-anchored tumour suppressor OPCML. Further, we demonstrate that AXL directly interacts with OPCML, preferentially so when AXL is activated by its ligand Gas6. As a consequence, AXL accumulates in cholesterol-rich lipid domains, where OPCML resides. Here, phospho-AXL is brought in proximity to the lipid domain-restricted phosphatase PTPRG, which de-phosphorylates the RTK/ligand complex. This prevents AXL-mediated transactivation of other RTKs (cMET and EGFR), thereby inhibiting sustained phospho-ERK signalling, induction of the EMT transcription factor Slug, cell migration and invasion. From a translational perspective, we show that OPCML enhances the effect of the phase II AXL inhibitor R428 *in vitro* and *in vivo*. We therefore identify a novel mechanism by which two spatially restricted tumour suppressors, OPCML and PTPRG, coordinate to repress AXL-dependent oncogenic signalling.

Introduction

Epithelial ovarian cancer (EOC) is one of the leading causes of cancer-related deaths in women across the world and the most lethal gynaecological malignancy [1]. Loco-regional dissemination of the tumour is deadly, with only 10–15% of patients surviving beyond 10 years [2]. Unfortunately, due to its relatively asymptomatic nature and early propensity to dissemination, EOC is typically diagnosed at late stage. Patients' tumours ultimately become resistant to existing treatments, and thus, there is an unmet need for alternative treatment strategies.

We have recently identified the receptor tyrosine kinase (RTK) AXL as a pivotal node of oncogenic RTK cross-talk in ovarian cancer [3,4]. AXL is an important driver of epithelial-to-mesenchymal transition (EMT) and tumour progression, and has been implicated in promoting cell adhesion, survival, proliferation, motility and invasion [5]. AXL is a member of the TAM subfamily of RTKs [6] with its only known ligand being growth arrest-specific-6 (Gas6). Binding of Gas6 to AXL results in homodimerisation of AXL in a 2:2 stoichiometry with Gas6 and subsequent activation of the AXL kinase domain [7]. In ovarian cancer, AXL overexpression confers worse prognosis [3] and it is primarily expressed during advanced-stage disease and at higher levels in peritoneal deposits and metastases compared to the primary tumour [8]. Silencing AXL in ovarian cancer cells abrogates peritoneal dissemination of the tumour, and additionally, inhibiting the Gas6/AXL pathway hinders further progression of established metastatic disease *in vivo* [9]. We have recently shown that the adversely prognostic mesenchymal subtype in ovarian cancer [10] presents sustained AXL signalling,

1 Department of Surgery and Cancer, Ovarian Cancer Action Research Centre, Imperial College London, London, UK
2 Cancer Science Institute of Singapore, National University of Singapore, Singapore, Singapore
3 NUS Graduate School for Integrative Sciences and Engineering, National University of Singapore, Singapore, Singapore
4 Division of Basic Science Research, Department of Systems Biology, The University of Texas MD Anderson Cancer Center, Houston, TX, USA
5 Department of Obstetrics and Gynecology, National University Health System, Singapore, Singapore
6 Institute of Molecular and Cell Biology, A*STAR (Agency for Science, Technology and Research), Singapore, Singapore
7 Department of Biochemistry, National University of Singapore, Singapore, Singapore
8 Early Clinical Development, IMED Biotech Unit, AstraZeneca, Cambridge, UK
*Corresponding author. Tel: +44 20 7594 2792; E-mail: h.gabra@imperial.ac.uk
**Corresponding author. Tel: +44 20 7594 1549; E-mail: c.recchi@imperial.ac.uk
†Present address: Institute for Stem Cell Biology and Regenerative Medicine, Stanford, CA, USA

which induces motility [3,11]. However, the mechanisms regulating AXL signalling remain unknown [12]. Given AXL is known to extensively transactivate other RTKs [3,13], identifying tumour suppressors that can repress these networks of oncogenic interactions would provide a promising platform for developing novel therapeutics.

Opioid-binding protein/cell adhesion molecule-like (OPCML) is a glycosylphosphatidylinositol (GPI)-anchored tumour suppressor that is silenced in over 83% of ovarian cancer patients by loss of heterozygosity (LOH) and epigenetic mechanisms [14] and correlates with poor patient progression-free survival in ovarian and breast cancers [15]. Hypermethylation of OPCML is also common in many other cancers such as lung, brain, breast, cervical, and gastrointestinal cancers and lymphomas, suggesting a conserved tumour suppressor function across various tissues and functional significance in their derived cancers [16]. We previously demonstrated that OPCML inhibits proliferation *in vitro* and abrogates tumorigenicity *in vivo* [14] by negatively regulating a repertoire of RTKs, such as EPHA2, FGFR1, FGFR3, HER2 and HER4 [15]. Hence, we sought to understand whether re-establishing this tumour suppressor would also repress other oncogenic drivers such as AXL in ovarian cancer.

Results

AXL overexpression-mediated impaired survival is mitigated by OPCML expression

First, we analysed the impact of AXL expression within the ICGC dataset of 154 patients [17]. AXL overexpression (above median) conferred a significantly worse overall survival in this dataset (HR = 1.997, $P = 0.0170$; Fig EV1A). In order to delineate the advantage of OPCML expression, we analysed the OPCML promoter methylation status in these patients. In the subset where there was gene promoter methylation of OPCML, AXL overexpression again demonstrated a significantly worse overall survival (HR = 1.929, $P = 0.0411$; Fig EV1B). However, in the cohort without OPCML promoter methylation, there was no such difference ($P = 0.1505$, non-significant; Fig EV1C). Furthermore, when considering the expression levels of AXL and OPCML using the CSIOVDB dataset for 1,868 EOC patients [18], a similar pattern was observed. AXL overexpression conferred significantly worse overall survival (HR = 1.335, $P = 0.0013$; Fig EV1D), and this was accentuated for patients with low expression of OPCML (HR = 1.431, $P = 0.0015$; Fig EV1E). However, in patients with high levels of OPCML, there was no significant difference between overall survival for AXL-low and AXL-high expression states (HR = 1.322, $P = 0.0651$; Fig EV1F).

In terms of progression-free survival from the TCGA, AXL overexpression (highest quartile) tended to confer worse prognosis (HR = 1.284, $P = 0.1030$, not significant; Fig EV1G), and this was significantly accentuated in patients with low OPCML expression (HR = 1.56, $P = 0.0419$; Fig EV1H). In patients with high levels of OPCML, the negative impact of AXL overexpression was reduced (HR = 1.12, $P = 0.5960$; Fig EV1I).

These findings suggest that the AXL overexpression-associated worsened prognosis could be mitigated by OPCML expression, underscoring the clinical and prognostic importance of OPCML. This

suggested that the tumour suppressor OPCML could modulate AXL signalling and so we explored this hypothesis.
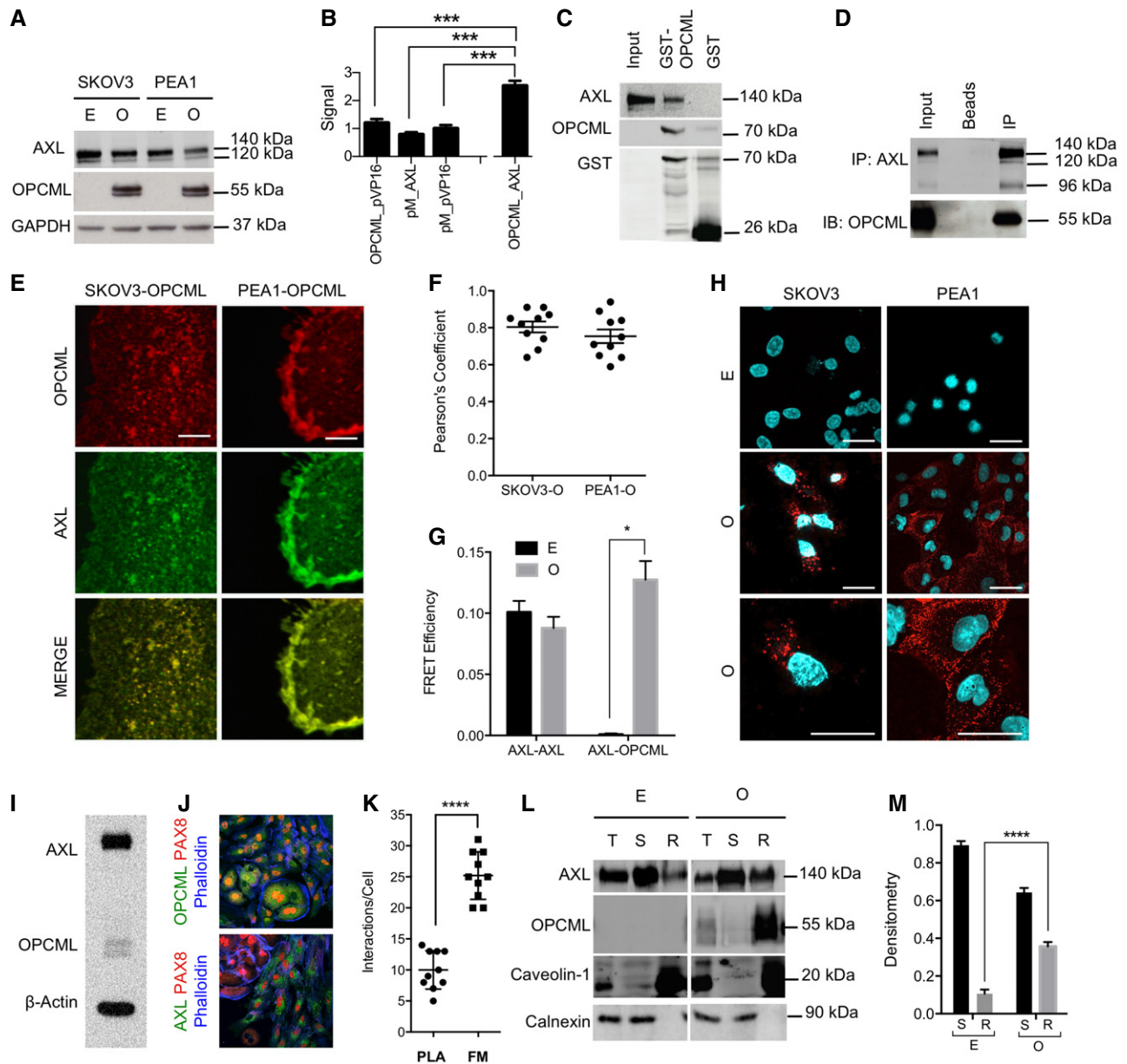
OPCML interacts with AXL

To assess whether OPCML could interact with and subsequently abrogate the oncogenic properties of AXL, we transduced AXL-expressing, OPCML-null (through somatic methylation) SKOV3 and PEA1 ovarian cancer cell lines with OPCML or the control (Empty) lentivirus to generate SKOV3-OPCML, SKOV3-Empty, PEA1-OPCML and PEA1-Empty cell lines, which were used in subsequent experiments (Fig 1A). In a mammalian 2-hybrid assay, a positive signal was detected in SKOV3-OPCML cells that express both AXL and OPCML (Fig 1B), suggesting for the first time an interaction between OPCML and AXL. A GST pull-down assay was also carried out using SKOV3-Empty cells, and AXL was detected in the eluate together with GST-OPCML (Fig 1C). The interaction between endogenous AXL and OPCML was also observed by co-immunoprecipitation in SKOV3-OPCML cells, where OPCML co-precipitated with AXL (Fig 1D).

The localisation of the proteins at the plasma membrane was analysed by immunofluorescence microscopy, and this revealed co-localisation between AXL and OPCML in both SKOV3-OPCML and PEA1-OPCML cells (Pearson's correlation $R = 0.804$ and 0.754, respectively, Fig 1E and F). This association was confirmed using Förster resonance energy transfer (FRET; Fig 1G), as well as *in situ* proximity ligation assay (PLA) Duolink (Fig 1H), both of which demonstrated a clear proximity between AXL and OPCML. The AXL-OPCML interaction was further confirmed in primary ovarian tumour cells expressing both AXL and OPCML (Fig 1I and J) using PLA (Fig 1K).

Since GPI-anchored proteins like OPCML are located in cholesterol-enriched lipid domains, which can be isolated as "liquid-ordered" detergent-resistant membrane (DRM) fractions, we also investigated the effect of the OPCML-AXL interaction on the membrane distribution of AXL. Upon fractionating the plasma membrane into DRM and the "liquid-disordered" detergent-soluble membrane (DSM) fraction, we observed that AXL was present in both compartments of the membrane in control cells lacking OPCML (Fig 1L). However, in cells expressing OPCML there was a shift in AXL localisation from the DSM to the DRM compartment where OPCML resides (Fig 1L and M), demonstrating that OPCML relocates AXL into cholesterol-enriched domains. To our knowledge, this is the first time that the interaction between OPCML and AXL and the subsequent AXL redistribution have been evidenced.

Gas6 stimulation promotes OPCML-AXL interaction, thereby altering AXL localisation and activation

To further understand the nature of the OPCML-AXL association, we decided to investigate how the binding of AXL to its ligand Gas6 would affect the functional interaction between AXL and OPCML. Given that the previous experiments were carried out in complete medium, which contains many growth factors, we used serum-free conditions to exclusively evaluate the effects of Gas6 addition. In serum-free non-stimulated conditions, we demonstrated that there was minimal co-localisation between AXL and OPCML in SKOV3-OPCML as observed by immunofluorescence staining (Pearson's correlation $R = 0.22$, Fig 2A and B). However, addition of

Figure 1. OPCML interacts with AXL.

A   Western blotting of AXL and OPCML protein levels in AXL-expressing, OPCML-null SKOV3 and PEA1 cell lines transduced with OPCML "O" or control Empty vector "E".

B   Mammalian 2-hybrid assay between OPCML and AXL.

C   Western blotting of the OPCML-GST pull down. Input: 1/20 of SKOV3-Empty whole-cell lysate.

D   Western blotting of the anti-AXL immunoprecipitation. Input: 1/100 of SKOV3-OPCML whole-cell lysate. IP, immunoprecipitated protein; IB, immunoblotted protein.

E   Immunostaining of OPCML (red) and AXL (green) in SKOV3-OPCML and PEA1-OPCML cells. Scale bar = 10 μm.

F   Pearson's correlation R for AXL-OPCML co-localisation in (E).

G   FRET efficiency for AXL-OPCML interaction in SKOV3-Empty "E" and SKOV3-OPCML "O", using AXL-AXL FRET as a positive control. Cells were labelled with anti-Axl rabbit (conjugated to donor probe) and anti-OPCML mouse (conjugated to acceptor probe), or anti-Axl mouse (conjugated to acceptor probe) and anti-Axl rabbit (conjugated to donor probe).

H   PLA of AXL-OPCML (red) in SKOV3 and PEA1 cells transduced with empty vector "E" or OPCML "O". Scale bar = 50 μm.

I, J   Primary ovarian tumour cells were characterised for AXL and OPCML levels by (I) Western blotting and (J) immunostaining. PAX8 was used to identify ovarian cancer cells.

K   Quantitation of AXL-OPCML PLA in primary cells. PLA = PLA secondary antibodies only. FM = primary antibodies anti-AXL and anti-OPCML plus PLA secondary antibodies. This assay was performed in full medium.

L   Western blotting of membrane fractionation of SKOV3-Empty cells: total cell lysate "T", liquid-disordered soluble fraction "S", detergent-resistant membrane fraction "R". Caveolin-1 is used as a marker of the R fraction, and Calnexin is used as a marker for the S fraction, E, SKOV3-Empty; O, SKOV3-OPCML.

M   Densitometry of AXL band intensities in (J) in S and R, normalised to AXL intensity in input.

Data information: Data are representative of at least three experiments with graphs depicting means ± SEM; (E) was performed once due to the limited numbers of primary cells; *$P < 0.05$, ***$P < 0.01$ and ****$P < 0.0001$ by Student's *t*-tests.

Gas6 strongly induced co-localisation within 30 min, and at 3 and 12 h, suggesting a sustained interaction between AXL and OPCML in the presence of the ligand (Pearson's correlation R = 0.68, 0.73, 0.83, respectively, Fig 2A and B). Interestingly, when we quantified this interaction using PLA, we found negligible association between the two proteins in non-stimulating conditions, but very strong and temporally progressive interaction upon addition of Gas6 (Fig 2C and D). This Gas6-induced AXL-OPCML interaction was also observed in primary ovarian tumour cells (Fig 2E), though the effect of serum starvation was limited probably due to the secretion of autocrine growth factors. Furthermore, we could observe an increase in the amount of OPCML immunoprecipitated with AXL upon Gas6 treatment, suggesting again that the addition of Gas6 increases the affinity between AXL and OPCML (Fig 2F). We additionally determined that this interaction also occurred between OPCML and the phosphorylated form of AXL (pAXL), as demonstrated by co-immunoprecipitation of OPCML by anti-pAXL (Fig 2G). A GST pull-down assay was also carried out, where pAXL was detected in the eluate together with GST-OPCML, again enhanced by Gas6 (Fig 2H). Thus, OPCML also binds to the active form of AXL upon Gas6 stimulation.

When we analysed the effect of Gas6 addition on AXL distribution by membrane fractionation in SKOV3-Empty, the total AXL protein was distributed between the DSM and DRM and this distribution remained constant over time (Fig 2I). Surprisingly, the pool of activated pAXL was detected almost exclusively in the DSM (Fig 2I). Interestingly, in SKOV3-OPCML the increased interaction between OPCML and AXL caused by the addition of Gas6 induced a progressive shift of AXL from the DSM into the DRM, where the GPI-anchored protein resides (Fig 2I and J). As a consequence, since in the DRM AXL is mostly not phosphorylated, the total levels of phosphorylated and activated AXL decreased in the presence of OPCML (Fig 2I).

As it is known that the association with lipid domain affects protein diffusion, we performed fluorescence recovery after photobleaching (FRAP) experiments on SKOV3-Empty and OPCML cells stimulated with Gas6 (Fig 2K). AXL recovery was less in SKOV3-OPCML cells, particularly upon Gas6 stimulation, compared to SKOV3-Empty cells (Fig 2K). The diffusion co-efficient dropped from 0.51 to 0.36 in SKOV3-OPCML cells upon Gas6 stimulation, while the reduction in SKOV3-Empty decreased from 0.66 to 0.57 (Fig 2L); this could be due to the increased association of AXL with the immobile lipid fraction upon Gas6 stimulation in SKOV3-OPCML (Fig 2M). To solidify our findings, FRET experiments were also performed to quantitate the level of AXL-OPCML interaction upon addition of Gas6 and a clear increase was observed at 30 min and 3 h (Fig 2N).

Given that OPCML continued to retain dephosphorylated AXL in the DRM, we analysed Gas6-stimulated cells for the presence of the ligand in the membrane fractions (Fig 2O). In the cells lacking OPCML, there were elevated AXL, pAXL and Gas6 in the DSM (Fig 2O). However in the presence of OPCML, Gas6 is sequestered in the DRM along with AXL, which is dephosphorylated, implying that, even though the RTK is still bound to its ligand, it has been deactivated (Fig 2O). This suggests that Gas6 serves to trigger as well as retain an enhanced OPCML-AXL interaction on the extracellular side of the plasma membrane, regardless of the intracellular phosphorylation status of the AXL kinase domain.

OPCML inhibits sustained Gas6/AXL signalling

Observing the changes in membrane distribution and activation status of AXL upon binding to OPCML, we sought to understand how OPCML would therefore affect the Gas6/AXL signalling cascade. In order to ascertain that Gas6-induced effects were exclusively through the AXL signalling node, AXL-depleted SKOV3 cells were stimulated with Gas6. Upon AXL depletion, Gas6 addition did not induce phosphorylation of AXL, or of AXL downstream effector molecules such as ERK (Fig EV2A), or motility (Fig EV2B and C), confirming that Gas6 activates the ERK pathway and motility exclusively through AXL in these tumour cells.

SKOV3-Empty and PEA1-Empty cell lines were stimulated with Gas6 over a 24-h time course. Gas6 induced the phosphorylation of AXL leading to sustained activation of ERK for up to 24 h (Fig 3A and B) and the induction of the EMT transcription factor Slug, a key factor in cell motility and invasiveness [19,20] (Fig 3A and B). OPCML expression reduced both the magnitude and the temporal duration of AXL phosphorylation and, interestingly, the temporal

Figure 2. Gas6 stimulation promotes OPCML-AXL interaction, thereby altering AXL localisation and activation.

A–D SKOV3-OPCML cells stimulated with Gas6 over a 12-h time course and (A) stained with DAPI (cyan), anti-OPCML (green) and anti-AXL (red) antibodies (scale bar = 10 µm), and (B) Pearson's correlation R was calculated; (C, D) OPCML-AXL interaction (red) was visualised by PLA (scale bar = 50 µm) and quantified, n = 3.

E Quantitation OPCML-AXL PLA interaction in primary ovarian tumour cells, n = 1. The six data points represent the quantifications from six separate images (from the same experiment).

F Co-immunoprecipitation with anti-AXL antibody in cells stimulated with Gas6 as indicated. Input: 1/50 of whole-cell lysate from SKOV3-OPCML cells. IP, immunoprecipitated protein; IB, immunoblotted protein.

G Co-immunoprecipitation with anti-pAXL antibody in SKOV3-OPCML cells stimulated with Gas6.

H OPCML-GST pull-down assay in SKOV3-Empty cells stimulated with Gas6.

I Membrane fractionation in SKOV3-Empty "E" and SKOV3-OPCML "O" cells into the detergent-resistant "R" membrane fraction and the detergent-soluble "S" fraction upon Gas6 stimulation.

J Ratio of AXL band intensity in "R" to total AXL "T" (T = S + R) from panel (I).

K–M (K) FRAP recovery curves. Black boxes represent median value, coloured boxes represent 1st–3rd quartile, and whiskers represent minimum to maximum values, (L) diffusion co-efficient and (M) percentage of AXL localised in insoluble lipid domain or soluble plasma membrane fraction in SKOV3-Empty "E" and SKOV3-OPCML "O" cells treated with Gas6.

N FRET efficiency in SKOV3-OPCML "O" cells stimulated with Gas6, and labelled with anti-Axl (donor probe) and anti-OPCML (acceptor probe).

O Western blotting of the "S" and "R" membrane fractions in SKOV3-Empty "E" and OPCML "O" cells stimulated with Gas6 for 3 h, for Gas6, AXL and pAXL.

Data information: Data are representative of at least three experiments with graphs depicting means ± SEM, (E) was performed once due to the limited numbers of primary cells; *P < 0.05, **P < 0.01, ***P < 0.001 and ****P < 0.0001 by Student's t-tests.

duration of the phospho-ERK (pERK) response in both cell lines, where pERK was completely abolished after 1–3 h post-Gas6 stimulation (depending on the cell line; Fig 3A and B). This observation

was confirmed using immunofluorescence staining to visualise the pERK response upon Gas6 treatment, and again, in the presence of OPCML, only transient phosphorylation of ERK was observed
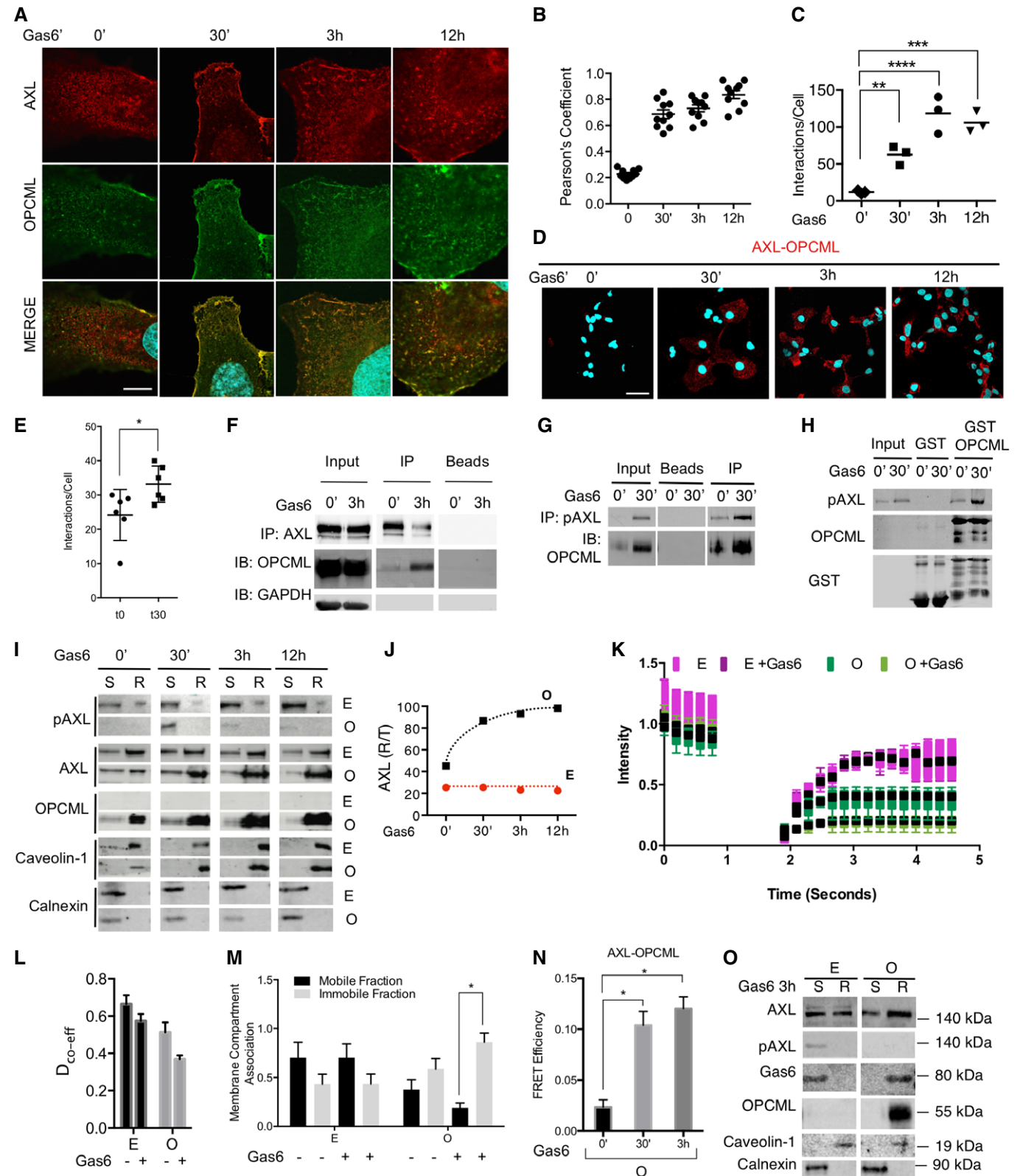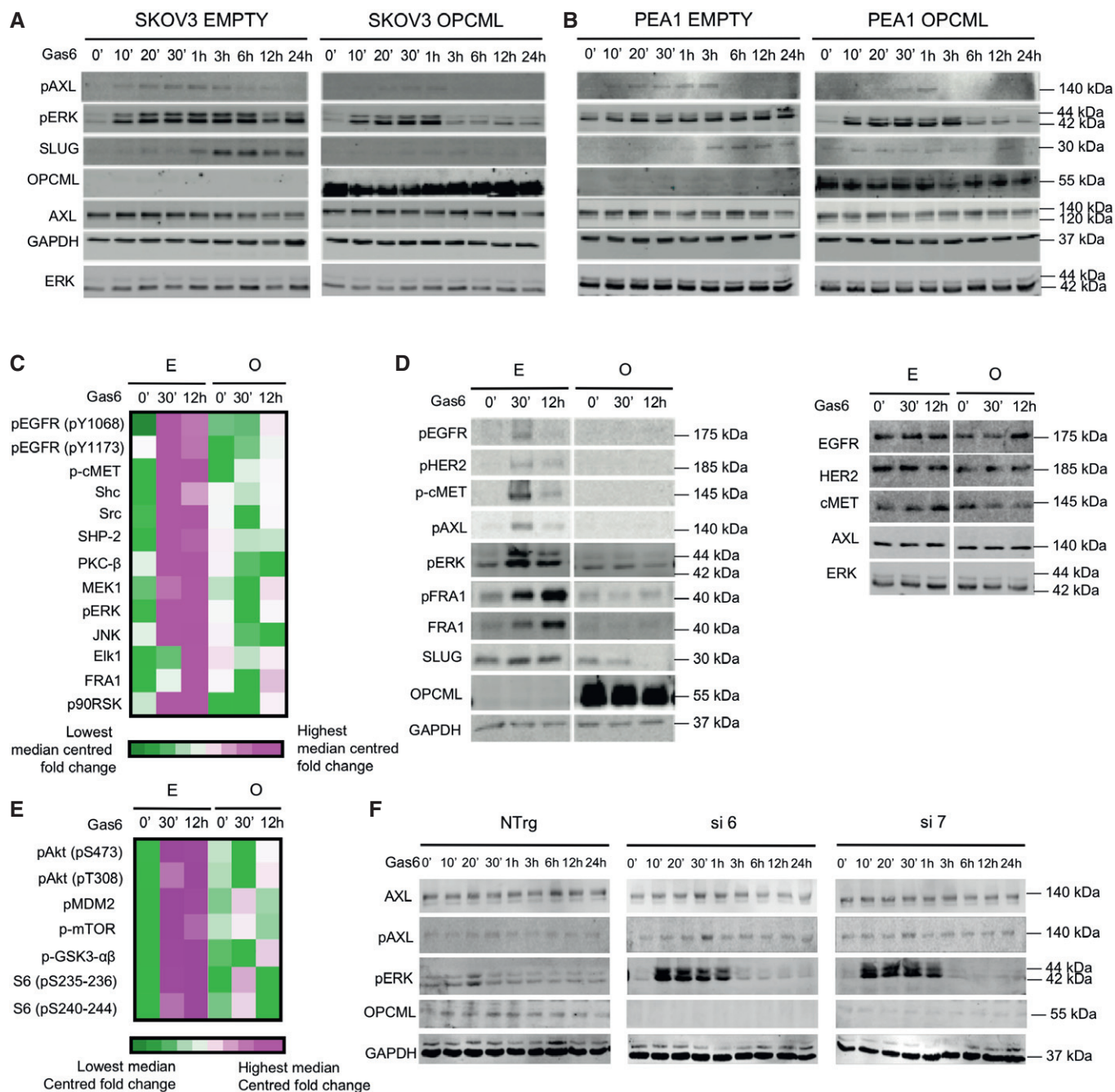

Figure 2.

Figure 3. OPCML represses oncogenic Gas6/AXL signalling.

A, B   SKOV3 (A) and PEA1 (B) (EMPTY and OPCML transduced) cell lines were serum starved and stimulated with Gas6 over a 24-h time course. GAPDH was used as a loading control.

C–E   (C, E) RPPA data showing phospho-RTK and downstream signalling moieties activated by Gas6/AXL stimulation in SKOV3-EMPTY and SKOV3-OPCML. Data are represented as Log2 normalised and median centred. The units of the colour key (green to magenta) represent −2.2 to +2.2 (Log2 normalised median centered). (D) Western Blotting of SKOV3-EMPTY and SKOV3-OPCML upon AXL activation. GAPDH was used as loading control.

F   Western blotting of non-targeting siRNA (NTrg)-, or siOPCML (si 6, si 7)-transfected FT190 cells stimulated with Gas6 over a 24-h time course. GAPDH was used as loading control.

Data information: Data in (A, B, D, F) are representative blots of at least three experiments. RPPA analysis was performed in triplicate.

(Fig EV2D and E). The repression of the sustained pERK response in OPCML-expressing cells had a profound effect in preventing Slug induction (Fig 3A and B).

To expand our understanding of the tumour suppressor effect of OPCML on the Gas6/AXL pathway at a systems level, reverse phase protein array (RPPA) was carried out on SKOV3-Empty and

SKOV3-OPCML cells. Upon Gas6 stimulation, we found elevated phospho-EGFR (pEGFR) and phospho-cMET (pMET) levels in SKOV3-Empty, both at 30 min and at 12 h (Fig 3C), analogous to the higher and sustained pAXL status observed previously by Western blotting, confirming the known cross-talk between AXL and other RTKs [3,21,22]. However, this effect was completely abolished in the presence of OPCML (Fig 3C), underscoring its potent tumour suppressor function. These results were also independently confirmed by Western blot (Fig 3D). A similar pattern was observed immediately downstream of the RTK network, with adapter proteins such as Shc, Src and Shp-2 displaying high phosphorylation levels in SKOV3-Empty treated with Gas6, but not in SKOV3-OPCML cells (Fig 3C). Further downstream in the signal cascade, MEK1, ERK and JNK demonstrated similar strongly induced phosphorylation status in SKOV3-Empty cells, which was abrogated by OPCML (Fig 3C), confirming the pERK dynamics observed above. The sustained phosphorylation of response proteins such as ELK1 [23], p90RSK [24] and FRA1 [25] at 12 h in SKOV3-Empty cells was also prevented by OPCML expression (Fig 3C and D). FRA1 activity has been linked to the induction of the EMT transcription factors ZEB1, Slug and motility [26–29], and this could explain the Slug induction observed in control cells upon Gas6 stimulation of AXL [3,11,30,31] and its consequent abrogation upon OPCML expression. Apart from the MAPK cascade, the RPPA analysis also revealed suppression of the AKT pathway by OPCML (Fig 3E). Therefore, functional proteomics clearly revealed the extent of suppression of pro-oncogenic signalling by OPCML at a systems level.

Silencing OPCML increases Gas6/AXL signalling in fallopian tube epithelial cells

Given that OPCML overexpression in ovarian cancer cell lines decreases oncogenic signalling, we examined whether silencing OPCML (Fig 3F) in the non-cancerous OPCML-expressing fallopian tube epithelial (FT190) cells [32] would show the opposite effect and amplify Gas6/AXL signalling.

Non-targeting siRNA-transfected FT190 showed minimal response to Gas6 stimulation with only a slight pERK response at 20 min. In contrast, OPCML-silenced cells showed a strong pERK response that persisted from 10 min until 1 h (Fig 3F). Hence, silencing OPCML in a non-cancer system amplified the Gas6/AXL signalling response, although over a shorter time

course than malignant SKOV3 or PEA1 cell lines, suggesting that AXL is likely to be under tighter regulation in non-cancerous systems.

OPCML inhibits Gas6/AXL-mediated increase in cancer cell motility and invasion

As AXL has been widely described for its role in stimulating cell migration and motility [33], we investigated how the suppression of AXL signalling by OPCML would affect Gas6/AXL-mediated motility in SKOV3 and PEA1 cells.

Both cell lines responded to Gas6 stimulation and showed a significant increase in kinetic parameters of motility, such as displacement and speed, compared to non-stimulated cells (Fig 4A and B). In contrast, OPCML-expressing cells showed no change in these parameters upon stimulation with Gas6, with displacement and speed values at the same levels as non-stimulated cells (Fig 4A and B).

We also analysed collective cell migration in both cell lines. Gap closure measurements showed that SKOV3-Empty and PEA1-Empty responded to Gas6 stimulation and rapidly closed the gap, while the untreated cells did not (Fig 4C–F). However, OPCML-expressing cells did not respond to Gas6 stimulation and showed no difference in collective cell migration compared to their untreated counterparts (Fig 4C–F). Migrating SKOV3-Empty cells had elevated pERK staining at 12 h upon Gas6 stimulation, while this was absent in SKOV3-OPCML cells (Fig EV3A), thus confirming our previous observations that OPCML blunts the pERK response to Gas6 and consequently prevents Gas6/AXL-mediated motility. To verify that it was indeed the MEK/ERK axis that was responsible for Gas6/AXL-induced motility, SKOV3-Empty cells were treated with the MEK inhibitor PD0325901 [34]. MEK inhibition did not prevent pAXL response, but abrogated pMEK, pERK, pFRA1 and Slug induction (Fig EV3B–D), as well as Gas6/AXL-induced motility (Fig EV3E–H).

To evaluate the effect of OPCML on cell invasion in a three-dimensional environment, SKOV3-Empty and SKOV3-OPCML cells were seeded as spheroids into a matrix of basement membrane extract. Compared to their untreated counterparts, Gas6-stimulated SKOV3-Empty spheroids showed peripheral invasive cells migrating into the matrix after 3 days, while OPCML-expressing cells remained unresponsive

Figure 4. OPCML abrogates Gas6/AXL-mediated increase in cell motility and invasion.

A–F   Single-cell tracking analysis upon stimulation with Gas6 over 12 h of Empty "E" or OPCML "O" (A) SKOV3 cells or (B) PEA1 cells. Gap closure assay and analysis of Empty "E" or OPCML "O" SKOV3 (C, D) and PEA1 (E, F) cells; dashed white lines represent initial boundary and scale bars = 200 μm.

G   Spheroid invasion assay of Empty "E" or OPCML "O" SKOV3 spheroids 72 h post-stimulation with Gas6. Scale bars = 1 mm.

H   Invasion from (G) was quantified and normalised to spheroid volume prior to the addition of chemotactic medium.

I   Western blotting of fallopian tube epithelial (FT190) cells transfected with non-targeting siRNA (NTrg) or two siRNA for OPCML (si 6 and si 7). GAPDH was used as loading control.

J   Analysis of Gas6-stimulated single-cell motility of FT190 cells transfected with siRNA for OPCML compared to non-targeting siRNA control.

K, L   (K) Western blotting of ovarian cancer cell lines PEO1, OVCA429, SKOV3, HEYA8 expressing different levels of AXL, and transduced with Empty vector control "E", or OPCML "O", and (L) densitometry.

M, N   Quantitation of gap closure assays of ovarian cancer cell lines PEO1, OVCA429, SKOV3, HEYA8 transduced with OPCML "O", or Empty vector control "E"; dashed white lines represent initial boundary and scale bars = 200 μm.

Data information: Data are representative of at least three experiments with graphs depicting means ± SEM: *$P < 0.05$, **$P < 0.01$, and ***$P < 0.001$ by Student's *t*-tests.
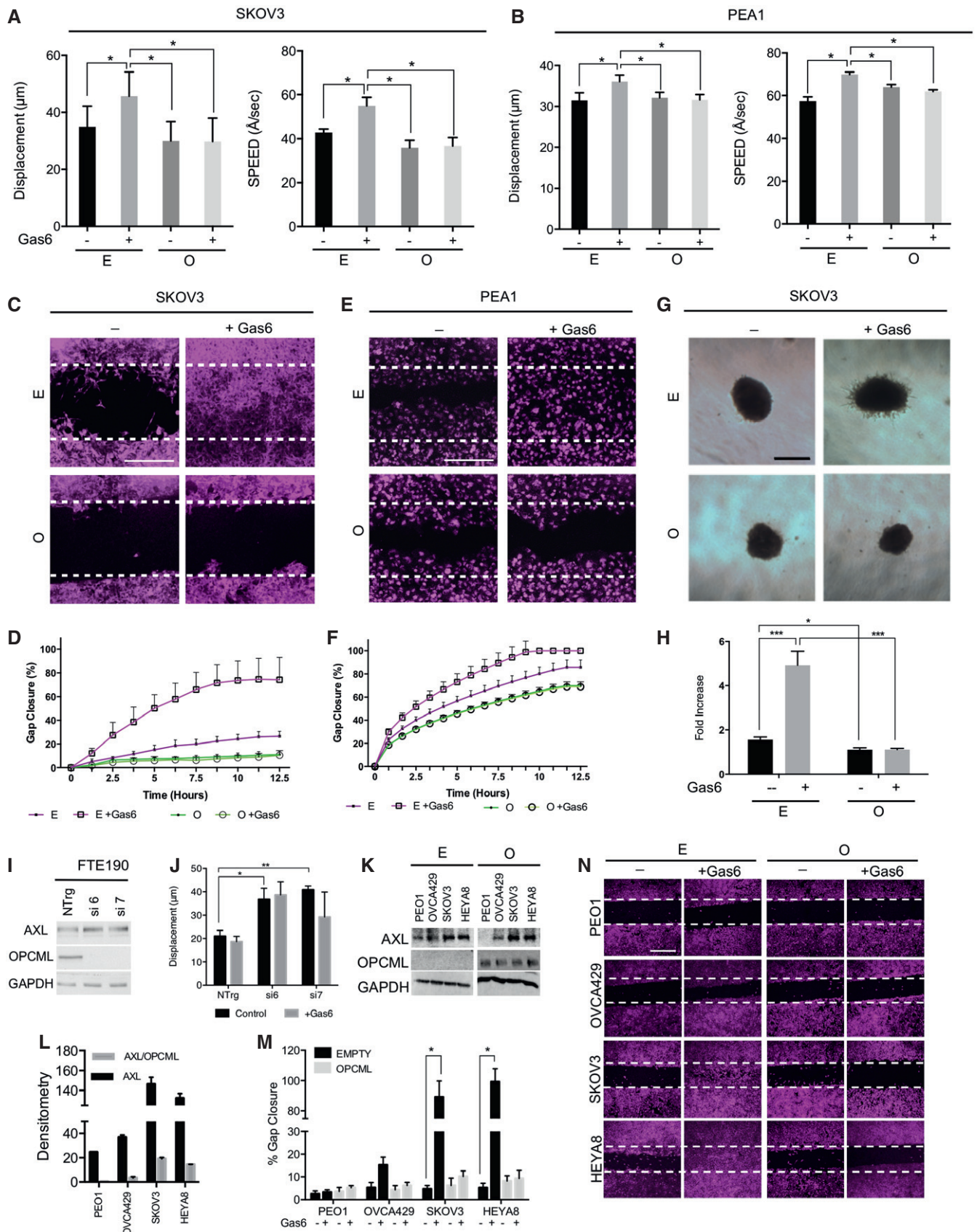
Figure 4.

to Gas6 stimulation (Fig 4G and H), underscoring the relevance of the tumour suppressor effect in a 3D microenvironment.

We also performed phenotypic assays with OPCML-silenced FT190 cells (Fig 4I). In single-cell motility assays, we demonstrated that siOPCML increased displacement compared to non-targeting siRNA-transfected FT190 (Fig 4J). However, as expected there was no further increase in motility in response to Gas6 stimulation (Fig 4J), as the pERK response to Gas6 was not sustained beyond 1 h (Fig 3F). We have previously shown that a sustained pERK response is required for Gas6-induced motility [3].

Furthermore, in order to assess whether OPCML-mediated suppression of AXL is possible for a range of AXL/OPCML ratios, we transduced ovarian cancer cell lines expressing different levels of AXL with OPCML (Fig 4K and L). In subsequent gap closure assays, it was evident that OPCML-mediated suppression of AXL-driven motility was achievable for a range of AXL/OPCML ratios (Fig 4L–N).

OPCML inhibits AXL directly, as well as the AXL-RTK network

As AXL has been shown to amplify its signalling via RTK cross-talk [3], we sought to examine the direct effect of OPCML on AXL inhibition by silencing HER2, EGFR and cMET. Cells depleted of HER2, EGFR and cMET still responded to Gas6 stimulation and showed increased gap closure compared to unstimulated control, but this was reduced compared to Gas6-driven motility in control cells; as expected, OPCML still suppressed this motility that was exclusively AXL driven (Fig EV4A–C). This implies that while OPCML can inhibit AXL in isolation, the drastic reduction in motility is evidenced by OPCML attenuating the AXL-RTK network.

Furthermore, as AXL tends to function in synergy with these RTKs, and given OPCML is a known regulator of RTK networks, we performed additional membrane fractionation experiments to evaluate the activation/inactivation of these RTKs upon OPCML modulation of AXL (Fig EV4D and E). In Gas6-stimulated conditions (Fig EV4D), or complete serum (Fig EV4E), the phosphorylated forms of the RTKs resided in the soluble membrane fraction, though to a reduced level in the OPCML-expressing cells. Upon Gas6 stimulation, in OPCML-expressing cells there was accumulation of total AXL, cMET, HER2 and EGFR into the insoluble membrane fraction, wherein phosphorylation could not be detected (Fig EV4D), while this RTK shift did not occur in control cells. This signifies that OPCML inhibition extends beyond AXL to also affect the AXL-driven RTK network.

Also, in order to compare the efficacy of OPCML suppression of AXL, motility of SKOV3 and PEA1 cells upon OPCML overexpression was compared to knockdown of AXL (Fig EV5A–C). Overexpressing OPCML in SKOV3 and PEA1 had the same effect in reducing motility as silencing AXL; furthermore, silencing AXL after OPCML overexpression did not further reduce motility, suggesting OPCML had already repressed AXL-driven motility (Fig EV5A–C). Similarly, in spheroid invasion assays, OPCML overexpression was comparable to AXL-knockdown (Fig EV5D and E). This suggests that the overexpression of OPCML has the same effect as silencing AXL. Also, no additional effect was evident upon silencing AXL in OPCML-overexpressing cells, suggesting that the tumour suppressor has already inhibited the AXL axis.

The integrity of cholesterol-enriched lipid domains is crucial for OPCML modulation of AXL signalling

In order to determine whether the change in compartmentalisation of AXL into cholesterol-enriched lipid domains is crucial for the suppressor action of OPCML, experiments were carried out to disrupt the integrity of the DRM.

Methyl-β-cyclodextrin (MBCD) was used to deplete cholesterol from the DRM and solubilise GPI-anchored and other transmembrane proteins into the DSM [35]. In SKOV3-OPCML cells, 30-min treatment with MBCD was sufficient to deplete cholesterol as evidenced by lack of cholesterol-bound Filipin staining [36] compared to the untreated control (Fig 5A). This cholesterol depletion lasted up to 12 h post-MBCD treatment (Fig 5A) and, as expected, induced a shift of OPCML and Caveolin-1 into the DSM (Fig 5B).

In SKOV3-OPCML cells, OPCML caused the accumulation of AXL in the DRM, but upon MBCD treatment, there was no such accumulation (Fig 5B and C). Therefore, perturbing cholesterol concentration prevented OPCML, and by extension, AXL, from accumulating in the DRM, the compartment where AXL resides in its dephosphorylated state. As a consequence, the levels of phosphorylated AXL remained high throughout the MBCD-treated Gas6-stimulated time course (Fig 5B–D) and the downstream signalling was restored in OPCML-expressing SKOV3 (Fig 5D–F). The pAXL and pERK activation persisted from the early time point of 30 min to 12 h in MBCD-treated SKOV3-OPCML cells, consistent with complete loss of function of OPCML upon disruption of cholesterol-enriched domains (Fig 5D–F).

Furthermore, we asked whether the loss of signalling suppression was exclusively due to disruption of the lipid domains, or possibly due to loss of interaction between AXL and OPCML. Interestingly, even upon loss of lipid domain integrity, AXL-OPCML interaction could still be visualised post-Gas6 stimulation (Fig 5G and H). This interaction rapidly reached maximal values at 30 min in the presence of MBCD and was retained until 12 h, unlike the control SKOV3-OPCML, where the AXL-OPCML interaction accumulated more slowly over time (Fig 5G and H). This could be due to enhanced mobility of OPCML through the membrane following the disruption of cholesterol-enriched domains, increasing the probability of binding activated AXL.

AXL sequestered in cholesterol-enriched domains by OPCML is dephosphorylated by PTPRG

We hypothesised that the OPCML-mediated change in membrane localisation of AXL could expose AXL to phosphatases that could dephosphorylate it. In order to identify a candidate phosphatase, we scrutinised the proteins that we had previously identified by proteomics of cholesterol-enriched domains [37] and we found only one tyrosine phosphatase, PTPRG, in the same membrane compartment as OPCML. We first performed a membrane fractionation and verified that PTPRG was located primarily in the DRM (Fig 6A). A co-immunoprecipitation with anti-AXL antibody showed a clear signal for interaction with PTPRG, but only in OPCML-expressing SKOV3 cells (Fig 6B). Subsequently, we performed PLA and FRET to determine the interaction between
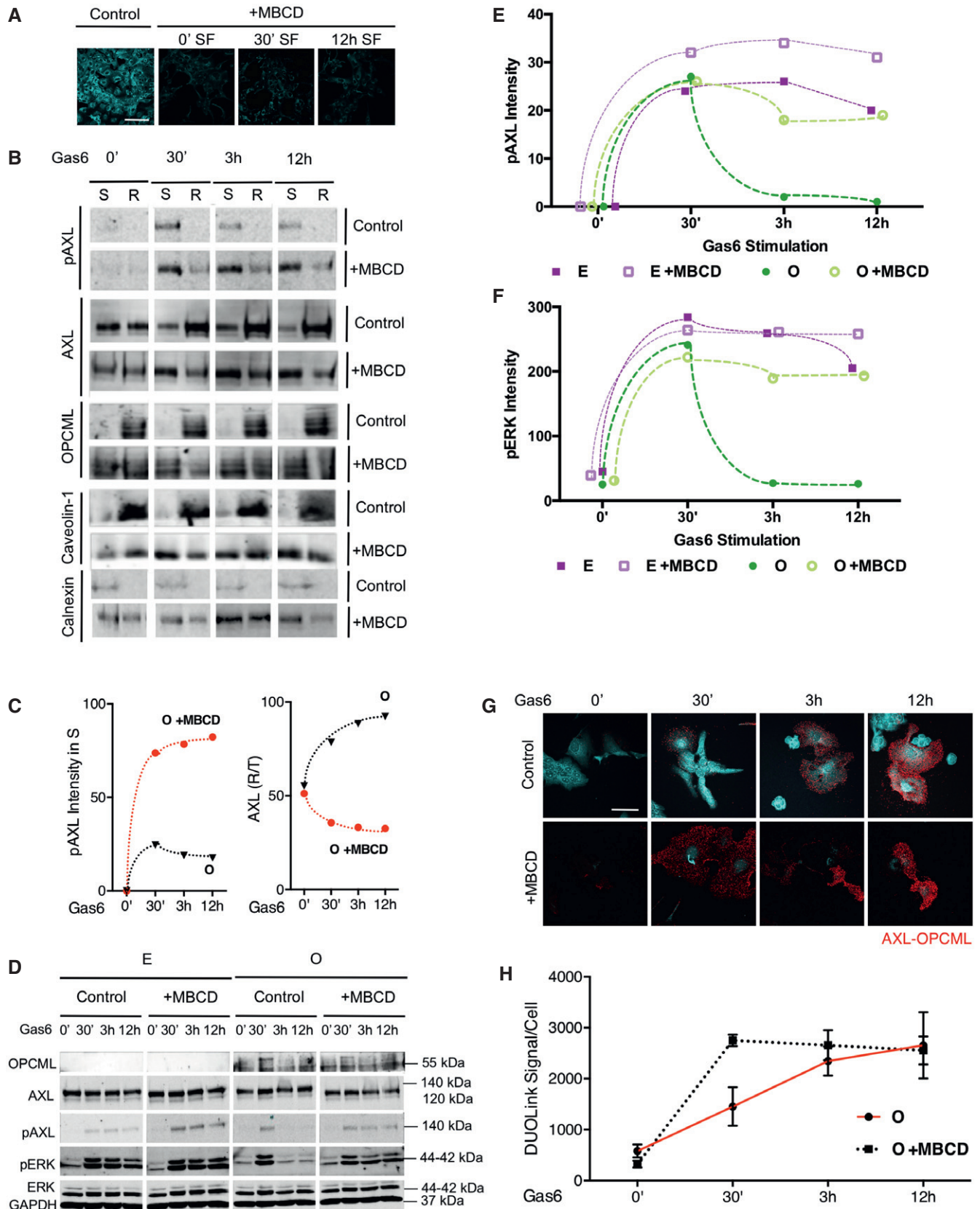
Figure 5.

◀

Figure 5.   The integrity of lipid domains is crucial for OPCML modulation of AXL signalling.

A   Filipin staining of SKOV3-OPCML cells treated for 30 min with 5 mM MBCD and allowed to recover for 0, 30 min and 12 h in serum-free (SF) medium. Scale bar = 50 μm.

B   Western blotting of SKOV3-OPCML cells treated with MBCD and separated into the detergent-resistant "R" membrane fraction and the detergent-soluble "S" fraction upon Gas6 stimulation.

C   Ratio of AXL band intensity in "R" or pAXL band intensity in "S" relative to total AXL "T" from SKOV3-OPCML "O" in (B).

D   MBCD treatment of SKOV3-Empty and SKOV3-OPCML cell lines was followed by the analysis of Gas6 signalling kinetics by Western blot. GAPDH was used as loading control.

E, F   Signalling kinetics are presented for pAXL and pERK in SKOV3-Empty "E" and SKOV3-OPCML "O", treated with MBCD and no treatment control, normalised to GAPDH, from (D).

G   PLA assay of AXL-OPCML interaction (red) upon Gas6 stimulation in both MBCD-treated and MBCD-non-treated SKOV3-OPCML cells. Scale bar = 50 μm.

H   Quantification of PLA signals from (G).

Data information: Data are representative of at least three experiments with graphs depicting means ± SEM.

AXL and PTPRG (Fig 6C and E). Interestingly, the expression of OPCML dramatically increased the interaction between AXL and PTPRG in both assays (Fig 6C and E). Furthermore, Gas6 stimulation, after serum starvation, increased the interaction between AXL and PTPRG only upon OPCML expression in both PLA and FRET (Fig 6D and F), demonstrating that the OPCML-mediated compartmentalisation of AXL in the DRM is crucial for the interaction of the kinase with the phosphatase. In order to validate the functionality of the AXL-PTPRG interaction, we silenced the phosphatase in SKOV3-Empty and SKOV3-OPCML cells (Fig 6G). As expected, siPTPRG did not have an effect on Gas6/AXL signalling in SKOV3-Empty cells as the RTK signals from the soluble fraction and is not modulated by the lipid domain-bound phosphatase (Fig 6G). However in SKOV3-OPCML cells, silencing PTPRG enabled sustained pAXL and consequently pERK signalling (Fig 6G), suggesting that OPCML represses AXL oncogenic signalling by promoting PTPRG access to the RTK. From our findings, we can conclude that OPCML blocks Gas6/AXL oncogenic signalling principally by stabilising AXL in the lipid domain fraction, where the raft-bound phosphatase PTPRG dephosphorylates pAXL (Fig 6H).

OPCML sensitises ovarian cancer cells to the AXL inhibitor R428 *in vitro* and *in vivo*

In order to investigate whether the OPCML-induced abrogation of signalling could translate into a potential clinical application, SKOV3-Empty and SKOV3-OPCML cells were treated with the AXL inhibitor R428 [38]. When we measured growth inhibition in R428-treated cells, we could observe that OPCML reduced the mean GI50 of R428 from 2.84 to 1.09 μM, resulting in a 2.6-fold decrease in the

dose of the inhibitor required for a GI50 effect (Fig 7A). Furthermore, in the presence of OPCML, cells showed attenuation of Gas6/AXL signalling at lower doses of R428 compared to control cells in both Western blot and immunofluorescence (Fig 7B and C). AXL, AKT and ERK phosphorylation were attenuated when SKOV3-Empty cells were incubated with R428 at 2.84 μM, but not at lower doses, while upon OPCML expression, Gas6/AXL signalling was curtailed at 1.09 μM of the drug (Fig 7B and C). This sensitisation to the AXL inhibitor could be a consequence of the combined effect of OPCML down-regulation of Gas6/AXL signalling and R428 inhibition of the catalytic kinase domain of AXL.

To translate the AXL signalling inhibition into a biologically relevant *in vivo* system, we chose the chick chorion allantoic membrane (CAM) assay; it would have been unfeasible to evaluate sensitisation in nude mice as OPCML completely suppresses tumour growth in this model [14]. SKOV3-Empty and SKOV3-OPCML cell lines were pre-incubated with R428, embedded in Matrigel, deposited on the CAM and allowed to form tumours. The *in ovo* findings substantiated the *in vitro* signalling inhibition results, with the SKOV3-Empty forming large tumours that were significantly suppressed with 2.84 μM, but less with 1.09 μM of R428 (Fig 7D and E). Interestingly, SKOV3-OPCML showed significant sensitisation to the lower concentration of R428 (Fig 7D and E). Of note, at 1.09 μM of R428, SKOV3-OPCML showed enhanced (approximately threefold) sensitisation to AXL inhibition, compared with SKOV3-Empty (Fig 7D and E).

The relative ratio of OPCML to AXL expression is predictive of patient overall survival in multiple cancers

In order to expand the clinical relevance of OPCML expression to different cancers, we analysed the relative amounts of OPCML to

Figure 6.   AXL sequestered in the lipid domains by OPCML is dephosphorylated by PTPRG.

A   Western blotting of the "S" and "R" membrane fractions in SKOV3-Empty "E" and OPCML "O" cells for PTPRG.

B   Western blotting of the anti-AXL immunoprecipitation in SKOV3-Empty "E" and OPCML "O" cells for AXL and PTPRG. Input: 1/100 of SKOV3-Empty or SKOV3-OPCML whole-cell lysate. IP, immunoprecipitated protein; IB, immunoblotted protein.

C, D   PLA assay of PTPRG-AXL interaction (red) in SKOV3-Empty "E" and OPCML "O" cells grown in (C) complete medium (scale bar = 50 μm), or (D) stimulated with Gas6 (scale bar = 50 μm).

E, F   FRET efficiency of AXL-PTPRG interaction in SKOV3-Empty "E", and SKOV3-OPCML "O" cells in (E) complete medium, or (F) Gas6-stimulated; cells were labelled with anti-Axl (donor probe) and anti-PTPRG (acceptor probe).

G   Western blotting of SKOV3-Empty "E" and OPCML "O" cells transfected with non-targeting siRNA (NTrg) or siRNA smartpool for PTPRG, stimulated with Gas6 over a 24-h time course. GAPDH was used as loading control.

H   Model of the mechanism of action of Gas6/AXL in cancer cells (left panel) and modulation by OPCML and PTPRG (right panel).

Data information: Data are representative of at least three experiments with graphs depicting means ± SEM: *P < 0.05, **P < 0.01, by Student's *t*-tests.

▶

Figure 6.

Figure 7.

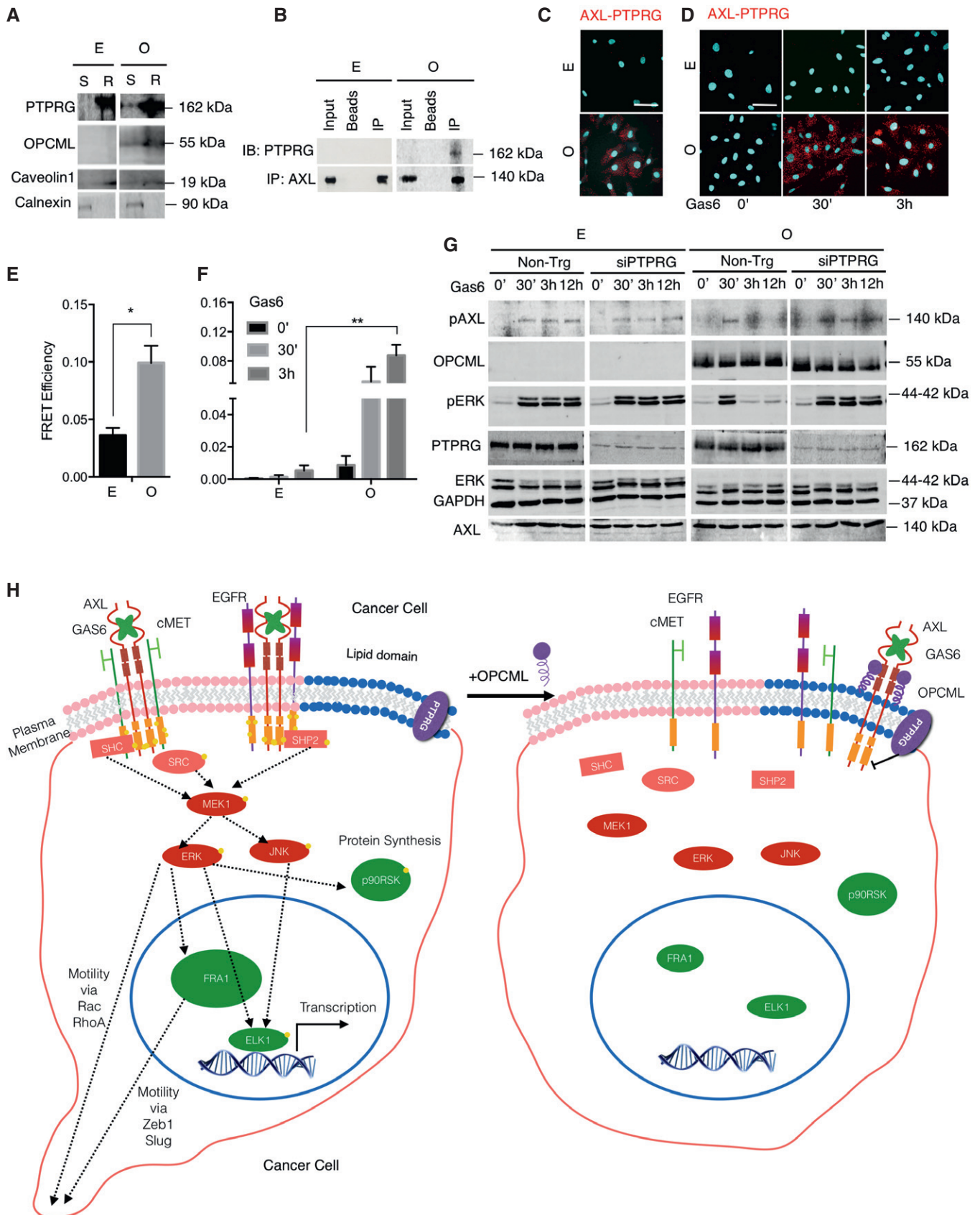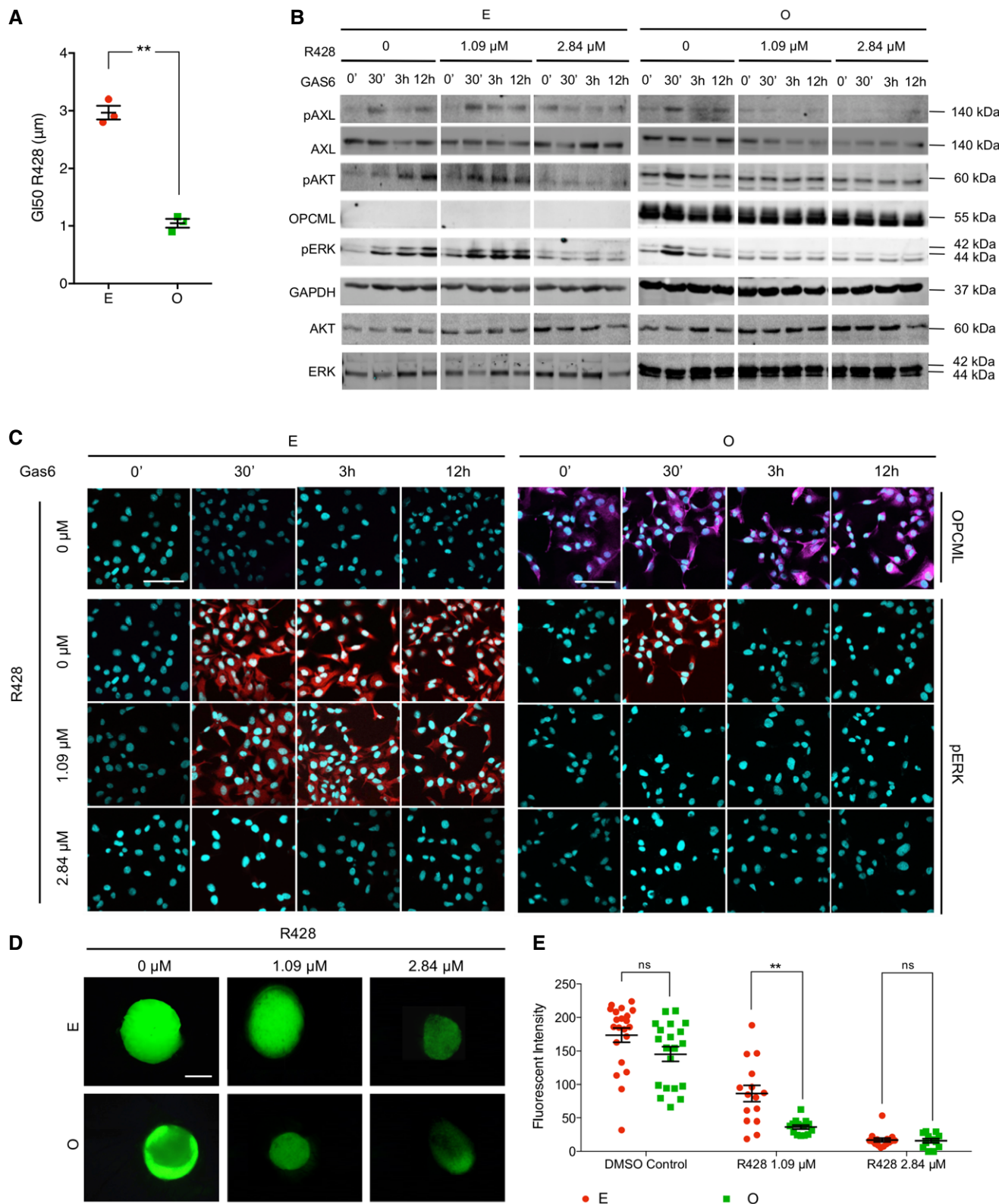AXL in different patient cohorts representing glioma, ovarian, lung, gastric, colorectal and renal cancers. In all these different cancer datasets, those patients with a high (above median) OPCML to AXL ratio had significant and substantial advantage in overall survival compared to patients with a low OPCML to AXL ratio (Fig 8A–L). This is representative of our *in vitro* observations, as the relative

Figure 7. OPCML potentiates the effects of the AXL inhibitor R428 *in vitro* and *in vivo*.

A Mean GI50 of SKOV3-Empty "E" and SKOV3-OPCML "O" cells upon R428 treatment.

B Western Blotting of SKOV3-Empty "E" and SKOV3-OPCML "O" cells pre-incubated with either no drug (DMSO only control), 1.09 μM R428 or 2.84 μM R428 for an hour and stimulated with Gas6 for the indicated times. GAPDH was used as loading control.

C Immunofluorescence staining of pERK (red) and OPCML (magenta) in SKOV3-Empty "E" and SKOV3-OPCML "O" cells treated with R428 and stimulated with Gas6 for the indicted time points. Scale bars = 50 μm.

D CAM assay of SKOV3-Empty "E" and SKOV3-OPCML "O" cells pre-treated with R428. Scale bars = 1 mm.

E Quantification of the fluorescence intensity of the tumours from (D).

Data information: Data are representative of at least three experiments with graphs depicting means ± SEM: n.s., not significant, **$P < 0.01$, Student's *t*-tests.

balance between the tumour suppressor OPCML and the oncogene AXL is crucial in determining effective tumour suppression or oncogene activation. A high OPCML/AXL ratio implies there are relatively more tumour suppressor moieties capable of modulating AXL into the lipid domains, while with a low OPCML/AXL ratio, there will be residual AXL signalling from the soluble fraction promoting oncogenesis.

Discussion

Ovarian cancer is a lethal gynaecological malignancy presenting with non-specific symptoms that delay detection. The resultant poor overall survival in the advanced disease state creates great unmet need to find therapeutically relevant targets to improve patient outcome. AXL has recently emerged as a promising therapeutic target in ovarian cancer [3,9] where it is overexpressed and confers poor prognosis [3,39,40]. However, the biology of AXL regulation remains to be elucidated, and understanding of these regulatory mechanisms will serve to identify novel targets and design appropriate drug candidates targeting relevant biology.

In this study, as a result of clinical insights suggesting a survival modulating link between AXL and OPCML, we found that Gas6-mediated AXL activation is profoundly diminished by the GPI-anchored tumour suppressor OPCML. The interaction between OPCML and AXL is enhanced in the presence of Gas6, as OPCML shows a higher affinity for AXL when bound to its ligand. This binding leads to the redistribution of AXL from the soluble membrane fraction to the cholesterol-rich, detergent-insoluble membrane compartment. As AXL accumulates into this compartment through its chaperone interaction with OPCML, we discovered that it is brought into close proximity with PTPRG, a phosphatase localised in cholesterol-enriched domains. PTPRG then dephosphorylates pAXL, thereby inactivating it. This suggests that, while typically the role of the ligand is to activate the RTK, in the presence of OPCML Gas6 ultimately leads to the inactivation of AXL by promoting the interaction with OPCML/PTPRG.

The change in AXL localisation by OPCML not only prevents the RTK downstream signalling, but also prevents AXL-mediated trans-activation of other RTKs such as EGFR and cMET, with which it has previously been shown to interact [3,21]. The dramatic reduction in AXL activation and RTK cross-talk abrogates downstream oncogenic responses from the Ras/MEK1/ERK and the PI3K-AKT pathways. This attenuation of the sustained oncogenic signalling prevents induction and activation of response proteins such as ELK1, p90RSK and FRA1. As a consequence, ERK/FRA1-induced cell motility [33] via the EMT transcription factor network involving ZEB1 [26,30] and Slug [31,41] is also profoundly inhibited. We have previously

shown that mesenchymal-type ovarian cancer cells, which have a potent response to Gas6 signalling in terms of motility and invasion, are characterised by a sustained pERK response, while epithelial-type ovarian cancer cells, which do not show increased motility in response to Gas6, present only a brief pERK activation [3]. The re-introduction of OPCML in mesenchymal-type ovarian carcinoma cells such as SKOV3 or PEA1 modifies the temporal pERK response to that of an epithelial-like signalling state, inhibiting the Gas6-mediated cellular motility response and abrogating the pERK/EMT pathway. Conversely, as expected, silencing OPCML in non-cancerous fallopian tube epithelial (FT190) cells increases the pERK response to Gas6/AXL signalling; however, in these "normal" cells siRNA inhibition is insufficient to stimulate motility as seen in the fully neoplastic state.

To our knowledge, this is the first report to describe the spatial constraint of AXL signalling in discrete membrane compartments, and how this can be affected by GPI-anchored proteins such as OPCML. Given that the liquid-disordered membrane fraction and the cholesterol-enriched fraction contain distinct subsets of proteins [42–45], the change in AXL membrane localisation from one compartment to the other exposes the RTK to phosphatases, such as PTPRG, which are specifically localised in cholesterol-enriched domains, resulting in dephosphorylation and inactivation of the AXL kinase domain. PTPRG has been previously shown to function as a strong tumour suppressor by repressing various oncogenic kinases in several cancers [46–51]. However, this is first time it has been shown to de-phosphorylate AXL. The novelty of the interaction between PTPRG and AXL is underscored by the requirement of an interacting partner such as OPCML to partition the RTK into a specific membrane compartment that facilitates exposure of activated AXL to the phosphatase. Given that OPCML may negatively regulate other RTKs directly as well as through cross-talk inhibition, a more general speculation is that OPCML may represent a master molecular "off" switch for many RTKs and thereby represent a negative regulator of RTK networks.

From a clinical perspective, we observed that a high OPCML/AXL ratio confers a better overall survival in patients affected by different types of cancer, underscoring the potentiality of developing therapeutic agents based on targeting OPCML/AXL pathways. Furthermore, similarly to what we have recently shown for HER2 and EGFR inhibitors [52], OPCML modulation of AXL signalling sensitises cancer cells to the AXL inhibitor R428, as evidenced by the dramatic decrease in signalling kinetics *in vitro* and the suppression of tumour growth *in ovo*. Likewise, given that AXL confers resistance to EGFR-targeted therapies [22,53,54] by diversifying signalling, as well as resistance to PI3K inhibitors due to association with EGFR [13], OPCML abrogation of AXL activation in synergy with such inhibitors could improve tumour responses without
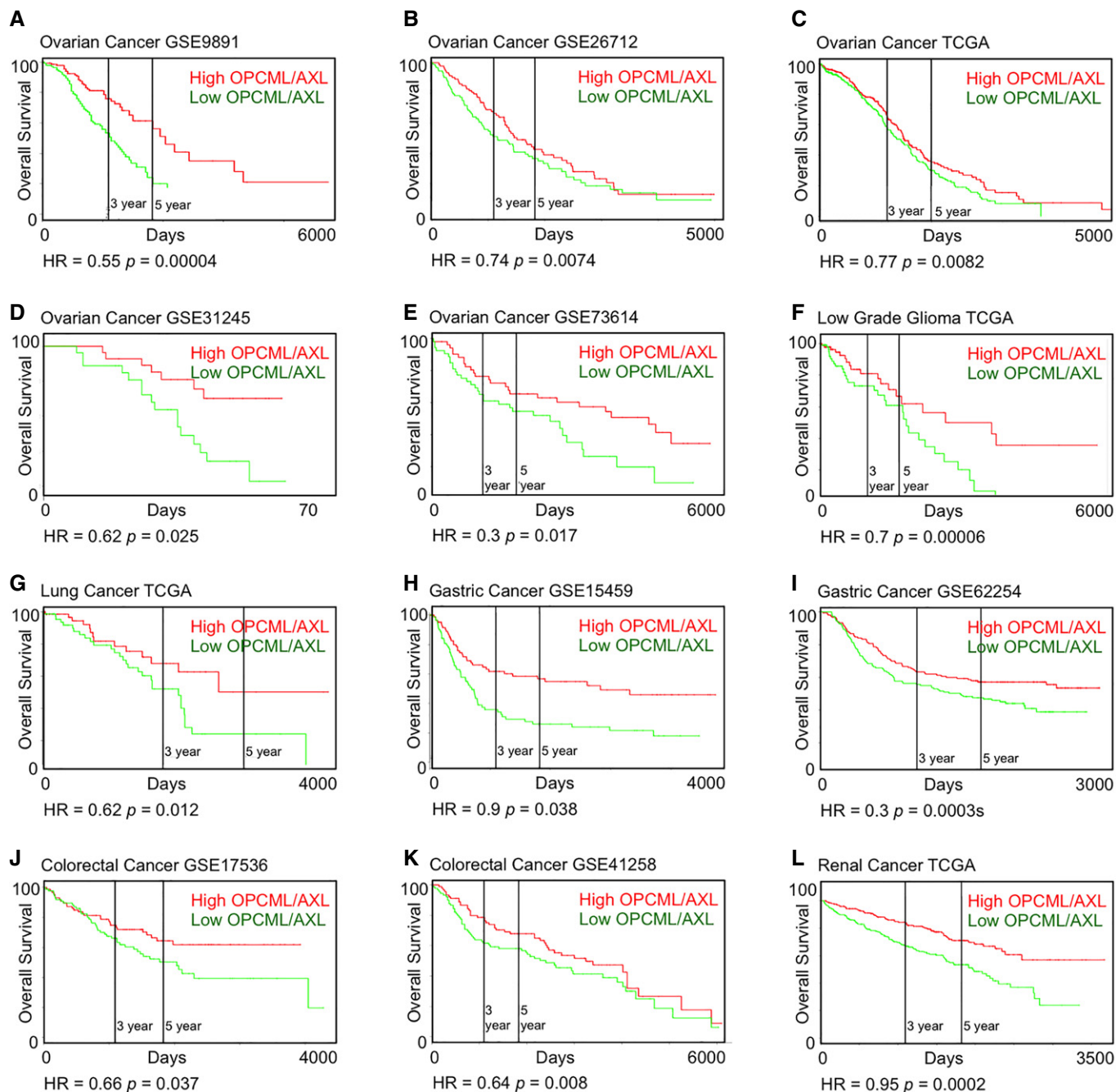
Figure 8. OPCML/AXL ratio is predictive of patient outcome *in silico*.

A–L   The relative ratio of OPCML to AXL was calculated, and above median values were defined as high OPCML/AXL (red), and below median values were defined as low OPCML/AXL (green). Kaplan–Meier curves showing overall patient survival of high OPCML/AXL and low OPCML/AXL cancer patient groups from (A) ovarian GSE9891, (B) ovarian GSE26712, (C) ovarian TCGA, (D) ovarian GSE31245, (E) ovarian GSE73614, (F) low-grade glioma TCGA, (G) lung TCGA, (H) gastric GSE15459, (I) gastric GSE62254, (J) colorectal GSE17536, (K) colorectal GSE41258, (L) renal TCGA. HR, Hazard ratio. Cox regression was used to calculate statistical significance.

enhancing treatment toxicity (as demonstrated by its limited impact on normal fallopian tube epithelial cells). Given the frequent methylation inactivation of OPCML, the development of mimetics to restore expression/function on the surface of cancer cells as extracellular tumour suppressor therapy represents a promising approach for cancer treatment and has been shown to induce tumour regression in mouse models [14,15]. Furthermore, the findings in this study suggest that OPCML-based therapeutics would be effective in modulation of RTK networks as opposed to linear systems. The effectiveness of disrupting nodes of oncogenic signalling would lie in minimising the bypass redundancy of RTK cross-talk, and this could represent an effective treatment strategy.

Materials and Methods

Cell culture

SKOV3, PEO1, OVCA429 and HEYA8 from ATCC and PEA1 from Cancer Research UK were cultured in RPMI 1640, 10% FBS, 1% penicillin and streptomycin (Sigma-Aldrich) and grown at 37°C in 5% CO_2. The fallopian tube epithelium cell line FT190 was a kind gift from the laboratory of Professor Ronny Drapkin, Dana Farber Cancer Institute, USA, and maintained in DMEM-Ham's F12 50/50 media, 1% penicillin and 2% Ultroser G serum substitute (Pall France SA).

Primary cell culture

At the time of cytoreductive surgery for advanced primary high-grade serous ovarian cancer, ovarian tumour was collected and immediately transferred to the laboratory for culturing. The project was performed under the Hammersmith and Queen Charlotte's and Chelsea Research Ethics Committee approval 05/QO406/178 and supplied by the Imperial College Healthcare NHS Trust Tissue Bank, following full patient consent. Primary tumour cells were isolated as described previously [55] and cultured in RPMI 1640, 20% FBS, 1% penicillin–streptomycin, 2 mM sodium pyruvate (Sigma) and 2.5 μg/ml insulin (Sigma).

shRNA-mediated AXL-knockdown

Validated AXL MISSION shRNA (TRCN0000001040 and TRCN0000001041) and control shRNA [sh-Luciferase targeting (#SHC007)] bacterial glycerol stocks were purchased from Sigma-Aldrich. Virus generated from transfected 293T cells was used to generate stable clones (selected and maintained with 5 μg/ml puromycin) for loss-of-function studies in experiments measuring invasion.

siRNA-mediated gene silencing

For siRNA-mediated AXL silencing in SKOV3 parental, SKOV3-OPCML-overexpressing and SKOV3-Control, and PEA1-OPCML-overexpressing and PEA1-Control cells, siAXL sequences (#J-003104-10, 12 13) from Dharmacon On-Target Plus were utilised along with a pooled non-targeting sequence (#D-001810-10-05). The siRNA transfection was carried as per manufacturer's protocol, at final concentration of 25 nM, and knockdown was evaluated at 48 h using immunoblotting. For loss of tumour suppressor function studies, siRNA-mediated OPCML silencing in FT190 cell lines was performed using siOPCML sequences (#J-011743-06, 07) from Dharmacon On-Target Plus along with the pooled non-targeting sequence.

Antibodies

AXL C89E7 rabbit mAb (#8661), phospho-AXL Tyr702 D12B2 rabbit mAb (#5724), phospho-AKT Ser473 D9E XP® rabbit mAb (#4060), phospho-AKT Thr308 D25E6 XP® rabbit mAb (#13038), AKT pan 11E7 rabbit mAb (#4685), GAPDH D16H11 XP® rabbit mAb (#5174), Slug C19G7 rabbit mAb (#9585), phospho-FRA1 Ser265 D22B1 rabbit mAb (#5841), phospho-HER2/Erb2 Tyr1248 rabbit mAb (#2247), HER2/Erb2 29D8 rabbit mAb (#2165), phospho-EGFR Tyr1068 D7A5 XP® rabbit mAb (#3777), phospho-Met Tyr1234/1235 3D7 rabbit mAb (#3129), and cMET 25H2 mouse mAb (#3127) were purchased from Cell Signaling Technology (CST). Phospho-ERK1 pT202/pY204+ phospho-ERK2 pT185/pY187 mouse mAb (ab50011), ERK1/2 rabbit pAb (ab17942), AXL mouse mAB (ab89224) were purchased from Abcam. EGFR/ErbB1 goat pAb (E1157) was bought from Sigma-Aldrich. OPCML goat pAb (AF2777) was obtained from R&D Systems. The above-listed primary antibodies were used in immunoblotting at 1:1,000 dilution.

OPCML mouse mAb (MAB27771, Clone 341723) from R&D Systems and the previously listed pERK and AXL antibodies were used 1:100 for immunostaining and Duolink.

AXL mouse mAB (ab89224) from Abcam and phospho-AXL Tyr691 (SAB4504605) from Sigma-Aldrich were used in Co-immunoprecipitation experiment of AXL and OPCML.

Western blotting

Whole-cell lysates were generated by lysis with RIPA buffer (#R0278, Sigma-Aldrich), along with protease (#539134) and phosphatase (#524625) inhibitor cocktails (Calbiochem, Boston, MA). BCA assay was used to evaluate protein concentrations (#23225, Thermo Scientific, Rockford, IL). SDS–PAGE gels were transferred onto PVDF membranes (#IPFL00010, Millipore, Billerica, MA). Membranes were blocked with Li-COR blocking buffer (#927-40000) and subsequently probed with primary antibodies diluted in 5% BSA/TBST, overnight at 4°C. Incubation with secondary antibodies containing fluorophores at 1:20,000 dilution (IRDye 800CW-conjugated goat anti-mouse #926-32210 or anti-rabbit #926-32211, IRDye 680-conjugated goat anti-mouse #926-32220 or anti-rabbit #926-32221, and IRDye 800CW-conjugated donkey anti-goat #926-32214 antibodies, LI-COR Biosciences, Lincoln, NE) enabled visualisation on the Odyssey Infrared Imaging System from LI-COR Biosciences.

Mammalian 2-hybrid

Assays were performed as described previously [52] with the extracellular domain of Axl cloned in the pVP16 vector downstream of the SV40 promoter and VP16 activation domain.

GST pull-down assay

Recombinant GST-OPCML proteins were utilised to study the binding of OPCML to target proteins. The GST-OPCML proteins were immobilised by Magne-GST™ Pull-Down System (Promega) through the GSH-linked magnetic particles and were incubated with cell lysates. Beads were then washed three times, and proteins were eluted by adding directly SDS sample buffer onto the particles and by boiling the sample for 5 min.

Co-immunoprecipitation assay

Co-immunoprecipitation experiments were carried out using the Pierce CO-IP Kit (#26149, Thermo Fisher Scientific) as per manufacturer's protocol. For the antibody immobilisation step, 50 μg of AXL mAb (ab89224) or 100 μg of pAXL pAb (SAB4504605) was diluted

onto the AminoLink Plus Coupling Resin. The cell lysates were precleared with control agarose resin, and co-immunoprecipitation was carried out by adding the precleared cell lysate to the antibody immobilised resin, with end-over-end-mixing at 4°C overnight. After elution, the sample was analysed by SDS–PAGE gel and followed by immunoblotting to detect protein–protein interaction.

Immunofluorescence microscopy

Cells were seeded on 13-mm glass coverslips in full medium and left to adhere for 24 h to reach 50% confluence. After the appropriate treatments, cells were fixed with ice-cold 100% methanol for 5 min at −20°C and then rehydrated thrice in PBS for 5 min each. Coverslips were blocked for 30 min with 3% BSA/PBS and then incubated with 1:100 dilution of primary antibodies in 1% BSA/PBS for 1 h in a moist environment. After three washes with PBS, cells were incubated with fluorophore labelled secondary antibodies (Alexa Fluorophores Life technologies, Donkey-anti-mouse Alexa Fluor® 488 R37114, Alexa Fluor® 546 A10036, Alexa Fluor® 680 A10038; Donkey-anti-rabbit Alexa Fluor® 488 R37118, Alexa Fluor® 546 A10040, Alexa Fluor® 680 A10043; or Donkey-anti-goat Alexa Fluor® 488 A11055, Alexa Fluor® 546 A11056, Alexa Fluor® 633 A21082) at 1:200 dilution in 1% BSA/PBS for 1 h. After three washes with PBS, the coverslips were mounted using ProLong® Gold Antifade Reagent with DAPI (Thermo Fisher Scientific) as mounting media. Images were taken with the SP5 Leica Confocal system.

Förster resonance energy transfer technique

FRET assay was performed using acceptor photobleaching method with proteins of interest being labelled with primary antibodies conjugated to FRET donor or acceptor probes using Lightning-Link® PE/Cy5 FRET Couples (SKU: 764-0010). Conjugation was performed as per manufacturer's protocol. Acceptor photobleaching was performed on SP5 Leica Confocal system according to prior established protocols [56], followed by calculation of FRET efficiency by determining increased donor signal intensity, normalised to acceptor photobleaching.

Duolink Proximity Ligation Amplification (PLA) assay

For PLA assay (Duolink, OLink Biosciences, Sigma-Aldrich #DUO92102, #DUO92104), the various cell lines were seeded on 13-mm glass coverslips. After the required treatments, the initial part of the immunofluorescence protocol was followed to label the fixed cells with primary antibodies from two different species (e.g., mouse anti-OPCML and rabbit anti-AXL). The rest of the protocol was followed as per manufacturer's instructions.

Membrane fractionation

Cells were grown in complete medium in a 150-cm dish to reach 80% confluence and osmotically lysed in a low salt buffer (20 mM Tris–HCl, pH 7.0) containing protease and phosphatase inhibitors. The cell suspension was passed through a 22-gauge needle three times, and an aliquot was retained for whole-cell lysate analysis. The cell suspension was centrifuged at 63,000 g (45,000 rpm) using an ultracentrifuge, for 1 h at 4°C. The membrane pellet was resuspended in ice-cold PBS plus inhibitors and centrifuged a second time at 45,000 rpm, for 30 min at 4°C. The membrane pellet was resuspended in ice-cold PBS, 1% Triton X-100, plus inhibitors and allowed to incubate for 30 min at 4°C. The detergent-treated membrane fraction was then centrifuged a third time at 45,000 rpm for 1 h at 4°C. The supernatant or the "disordered" detergent-soluble membrane fraction (DSM) was removed and retained for analysis. The remaining pellet or the "ordered" detergent-resistant insoluble membrane fraction (DRM) was solubilised in 1% SDS. The DRM was resuspended in a volume of 1% SDS equal to the volume of DSM.

Kinetic stimulation studies with Gas6

The cell lines were seeded to attain 70% confluence, serum starved overnight and activated with 400 ng/ml Gas6 (#885-GS, R&D Systems) for 0, 10, 20, 30 min, 1, 3, 6, 12 and 24 h, and lysates were collected for analysis.

Fluorescence Recovery After Photobleaching (FRAP) measurements and analysis

Mouse anti-Axl Fab was fluorescently conjugated and used to label SKOV3 cells at 37°C for 0.5 h. A circular spot, covering up to 1% of the surface area of the cell, was bleached with high laser power, and the subsequent recovery of fluorescence was recorded with 1/100-1/50 of the bleaching laser power for 4 min. FRAP recordings were carried out in CO_2-independent medium (Gibco) with 10% FBS on the SP5 Leica Confocal live imaging microscope at 37°C. The experimental data were corrected for bleaching occurring during recording, normalised to a prebleach fluorescence intensity and fitted to a 2D diffusion model. The theoretical fit adjusted the characteristic recovery time, the postbleach fluorescence intensity immediately after photobleaching and the fluorescence intensity at infinite time after photobleaching. The apparent diffusion co-efficient, D (calculated from the characteristic recovery time), and the fraction recovered were derived from the theoretical fits for every experiment and subsequently averaged. This protocol was adapted from previously established techniques [57].

Reverse phase protein array (RPPA)

The cell lines were serum starved overnight and treated with 400 ng/ml Gas6 for 0, 30 min or 12 h. Whole-cell lysates were generated by lysis with RIPA buffer, along with protease and phosphatase inhibitor cocktails.

RPPA procedure involved serial dilution of samples and subsequent colorimetric detection by antibodies upon tyramide dye amplification [58]. Spot intensity assessment was using R package developed in-house at MD Anderson Cancer Center with protein levels being quantified by SuperCurve method (http://bioinformatics.mdanderson.org/OOMPA). Data were log-transformed (base 2) and median-control normalised across all proteins within a sample.

Single-cell motility tracking

The cell lines were seeded at 50% confluence in ibidi 24-well plate and serum starved overnight. They were stained for an hour with

Hoechst nuclear dye (Life Technologies #62249, 1:500,000) for an hour and then stimulated with 400 ng/ml Gas6, while control cells were left untreated and visualised under the SP5 Leica Confocal system overnight at intervals of 10 min. The results were analysed with ImageJ software using Trackmate® to calculate kinetic parameters.

Gap closure assays

The cell lines were seeded at 100% confluence into culture inserts (Ibidi #80209) in a 24-well plate and serum starved overnight. Cell Mask membrane dye (Life Technologies #C10049, 1:4,000) was added for an hour, the insert removed to generate a 500-μm gap and stimulated with 400 ng/ml Gas6. Control cells were not stimulated. The cells were visualised under the SP5 Leica Confocal system overnight at intervals of 10 min. The results were analysed with ImageJ software to generate the gap closure at 12 h post-Gas6 stimulation.

Spheroid invasion assay

Five thousands cells were seeded in a Cultrex® 96-Well Kit (3D Spheroid BME Cell Invasion Assay, Trevigen, #3500-096-K), and the assay was performed as per manufacturer's protocol. The spheroids were grown under normal cell culture condition at 37°C and 5% CO_2, and invasion was monitored over a period of time. Results were documents on Day 3.

Cholesterol depletion

Methyl-β-cyclodextrin (MBCD, #C4555, Sigma-Aldrich) was used to deplete cholesterol. SKOV3-OPCML cells were grown on 13-mm coverslips and treated with 5 mM MBCD for 30 min at 37°C; control cells were maintained without cholesterol depletion. Following MBCD treatment, cells were allowed to recover for 0, 30 min and 12 h in serum-free medium, then fixed with ice-cold methanol for 5 min and rehydrated thrice with PBS. The cells were stained with 0.05 mg/ml filipin (#C4767, Sigma-Aldrich) diluted in PBS for 1 h at room temperature and rinsed thrice with PBS. The coverslips were mounted in non-DAPI mounting medium, and the filipin staining was observed under the 405 nm wavelength of a fluorescent microscope.

AXL inhibitor studies

The cell lines were seeded so as to obtain 80% confluence at the end of study, incubated with R428 (Selleckchem, #BGB324) at varying doses between 0 and 80 μM for 48 h to calculate GI50 doses. Cell Titer MTS cell proliferation assay (Promega #G3580) was used to evaluate 50% growth inhibition.

Chick Chorion Allantoic Membrane (CAM) model

All the procedures involving chicken embryos were performed in agreement with community and national legislation (Directive 2010/63/EU; Animals Scientific Procedures Act 1986) and also in agreement with the Basel Declaration. The procedure received prior approval by the competent National Authority (project licence:

PPL70/7997) and by Imperial College's Animal Welfare and Ethical Review Body.

Fertilised chicken eggs were purchased from Henry Stewart & Co. Ltd (Fakenham, UK) cleaned and incubated at 37°C with 55% relative humidity on embryonic day (ED) 1, and CAM assay was performed according to established protocols [59]. Between ED7 and ED10, 10^6 cells in 100 μl Matrigel (BD Biosciences) were inoculated onto the membranes. Tumour growth and viability of the embryo were checked daily. Tumour dimensions were measured using SteREO Discovery.V8 microscope (Zeiss, Germany) with Zen 2.0 blue edition software (Zeiss).

Statistical analysis

Statistical analyses were conducted using Matlab ® R2012a version 7.14.0.739 and statistics toolbox version 8.0 (MathWorks; Natick, MA). Kaplan–Meier analyses were conducted using GraphPad Prism ® version 5.04 (GraphPad Software; La Jolla, CA). Statistical significance of the Kaplan–Meier analysis was calculated by log-rank test. Gaussian distribution and variance equality of the data were verified.

Expanded View for this article is available online.

Author contributions

Conceptualisation: JA, RY-JH, JPT, CR and HG; Methodology: AP, MA and YJ; Formal Analysis: JA and TZT; Investigation: JA, EZ, EK, ZK and SR-N; Resources: GBM, PC, KN and CF; Writing—Original Draft: JA, CR and HG; Writing—Review and Editing: GBM, RH and JPT; Visualisation: JA; Supervision: CR and HG; Project Administration: JA and CR; Funding Acquisition: JA and HG.

Conflict of interest

H. Gabra is a VP head of Oncology Clinical Discovery (concurrent position with his Imperial tenured chair in medical oncology) in AstraZeneca and has ownership interest (including patents) to develop OPCML-based therapeutics. No potential conflict of interests were disclosed by the other authors.

References

1. Siegel R, Ma J, Zou Z, Jemal A (2014) Cancer statistics, 2014. *CA Cancer J Clin* 64: 9–29
2. Naora H, Montell DJ (2005) Ovarian Cancer Metastasis: integrating insights from disparate model organisms. *Nat Rev Cancer* 5: 355–366
3. Antony J, Tan TZ, Kelly Z, Low J, Choolani M, Recchi C, Gabra H, Thiery JP, Huang RY (2016) The GAS6-AXL signaling network is a mesenchymal

(Mes) molecular subtype-specific therapeutic target for ovarian cancer. *Sci Signal* 9: ra97

4. Halmos B, Haura EB (2016) New twists in the AXL(e) of tumor progression. *Sci Signal* 9: fs14

5. Graham DK, DeRyckere D, Davies KD, Earp HS (2014) The TAM family: phosphatidylserine sensing receptor tyrosine kinases gone awry in cancer. *Nat Rev Cancer* 14: 769–785

6. Linger RMA, Keating AK, Earp HS, Graham DK (2008) TAM receptor tyrosine kinases: biologic functions, signaling, and potential therapeutic targeting in human cancer. *Adv Cancer Res* 100: 35–83

7. Stitt TN, Conn G, Gore M, Lai C, Bruno J, Radziejewski C, Mattsson K, Fisher J, Gies DR, Jones PF *et al* (1995) The anticoagulation factor protein S and its relative, Gas6, are ligands for the Tyro 3/Axl family of receptor tyrosine kinases. *Cell* 80: 661–670

8. Brodsky AS, Fischer A, Miller DH, Vang S, MacLaughlan S, Wu HT, Yu J, Steinhoff M, Collins C, Smith PJ *et al* (2014) Expression profiling of primary and metastatic ovarian tumors reveals differences indicative of aggressive disease. *PLoS One* 9: e94476

9. Rankin EB, Fuh KC, Taylor TE, Krieg AJ, Musser M, Yuan J, Wei K, Kuo CJ, Longacre TA, Giaccia AJ (2010) AXL is an essential factor and therapeutic target for metastatic ovarian cancer. *Can Res* 70: 7570–7579

10. Tan TZ, Miow QH, Huang RY, Wong MK, Ye J, Lau JA, Wu MC, Bin Abdul Hadi LH, Soong R, Choolani M *et al* (2013) Functional genomics identifies five distinct molecular subtypes with clinical relevance and pathways for growth control in epithelial ovarian cancer. *EMBO Mol Med* 5: 983–998

11. Al-Hajj M, Wicha MS, Benito-Hernandez A, Morrison SJ, Clarke MF (2003) Prospective identification of tumorigenic breast cancer cells. *Proc Natl Acad Sci USA* 100: 3983–3988

12. Antony J, Huang RY (2017) AXL-driven EMT state as a targetable conduit in cancer. *Cancer Res* 77: 3725–3732

13. Elkabets M, Pazarentzos E, Juric D, Sheng Q, Pelossof RA, Brook S, Benzaken AO, Rodon J, Morse N, Yan JJ *et al* (2015) AXL mediates resistance to PI3Kalpha inhibition by activating the EGFR/PKC/mTOR axis in head and neck and esophageal squamous cell carcinomas. *Cancer Cell* 27: 533–546

14. Sellar GC, Watt KP, Rabiasz GJ, Stronach EA, Li L, Miller EP, Massie CE, Miller J, Contreras-Moreira B, Scott D *et al* (2003) OPCML at 11q25 is epigenetically inactivated and has tumor-suppressor function in epithelial ovarian cancer. *Nat Genet* 34: 337–343

15. McKie AB, Vaughan S, Zanini E, Okon IS, Louis L, de Sousa C, Greene MI, Wang Q, Agarwal R, Shaposhnikov D *et al* (2012) The OPCML tumor suppressor functions as a cell surface repressor-adaptor, negatively regulating receptor tyrosine kinases in epithelial ovarian cancer. *Cancer Discov* 2: 156–171

16. Cui Y, Ying Y, van Hasselt A, Ng KM, Yu J, Zhang Q, Jin J, Liu D, Rhim JS, Rha SY *et al* (2008) OPCML is a broad tumor suppressor for multiple carcinomas and lymphomas with frequently epigenetic inactivation. *PLoS One* 3: e2990

17. International Cancer Genome Consortium, Hudson TJ, Anderson W, Artez A, Barker AD, Bell C, Bernabe RR, Bhan MK, Calvo F, Eerola I *et al* (2010) International network of cancer genome projects. *Nature* 464: 993–998

18. Tan TZ, Yang H, Ye J, Low J, Choolani M, Tan DS, Thiery JP, Huang RY (2015) CSIOVDB: a microarray gene expression database of epithelial ovarian cancer subtype. *Oncotarget* 6: 43843–43852

19. Cobaleda C, Perez-Caro M, Vicente-Duenas C, Sanchez-Garcia I (2007) Function of the zinc-finger transcription factor SNAI2 in cancer and development. *Annu Rev Genet* 41: 41–61

20. De Craene B, Berx G (2013) Regulatory networks defining EMT during cancer initiation and progression. *Nat Rev Cancer* 13: 97–110

21. Gujral TS, Karp RL, Finski A, Chan M, Schwartz PE, MacBeath G, Sorger P (2013) Profiling phospho-signaling networks in breast cancer using reverse-phase protein arrays. *Oncogene* 32: 3470–3476

22. Meyer AS, Miller MA, Gertler FB, Lauffenburger DA (2013) The receptor AXL diversifies EGFR signaling and limits the response to EGFR-targeted inhibitors in triple-negative breast cancer cells. *Sci Signal* 6: ra66

23. Ebisuya M, Kondoh K, Nishida E (2005) The duration, magnitude and compartmentalization of ERK MAP kinase activity: mechanisms for providing signaling specificity. *J Cell Sci* 118: 2997–3002

24. Hauge C, Frodin M (2006) RSK and MSK in MAP kinase signalling. *J Cell Sci* 119: 3021–3023

25. Vial E, Marshall CJ (2003) Elevated ERK-MAP kinase activity protects the FOS family member FRA-1 against proteasomal degradation in colon carcinoma cells. *J Cell Sci* 116: 4957–4963

26. Shin S, Blenis J (2010) ERK2/Fra1/ZEB pathway induces epithelial-to-mesenchymal transition. *Cell Cycle* 9: 2483–2484

27. Thiery JP (2002) Epithelial-mesenchymal transitions in tumour progression. *Nat Rev Cancer* 2: 442–454

28. Thiery JP, Sleeman JP (2006) Complex networks orchestrate epithelial-mesenchymal transitions. *Nat Rev Mol Cell Biol* 7: 131–142

29. Yang J, Weinberg RA (2008) Epithelial-mesenchymal transition: at the crossroads of development and tumor metastasis. *Dev Cell* 14: 818–829

30. Bakiri L, Macho-Maschler S, Custic I, Niemiec J, Guio-Carrion A, Hasenfuss SC, Eger A, Muller M, Beug H, Wagner EF (2015) Fra-1/AP-1 induces EMT in mammary epithelial cells by modulating Zeb1/2 and TGFbeta expression. *Cell Death Differ* 22: 336–350

31. Lee Y, Lee M, Kim S (2013) Gas6 induces cancer cell migration and epithelial–mesenchymal transition through upregulation of MAPK and Slug. *Biochem Biophys Res Comm* 434: 8–14

32. Karst AM, Drapkin R (2012) Primary culture and immortalization of human fallopian tube secretory epithelial cells. *Nat Protoc* 7: 1755–1764

33. Vial E, Sahai E, Marshall CJ (2003) ERK-MAPK signaling coordinately regulates activity of Rac1 and RhoA for tumor cell motility. *Cancer Cell* 4: 67–79

34. Chua KN, Sim WJ, Racine V, Lee SY, Goh BC, Thiery JP (2012) A cell-based small molecule screening method for identifying inhibitors of epithelial-mesenchymal transition in carcinoma. *PLoS One* 7: e33183

35. Ilangumaran S, Hoessli DC (1998) Effects of cholesterol depletion by cyclodextrin on the sphingolipid microdomains of the plasma membrane. *Biochem J* 335(Pt 2): 433–440

36. Robinson JM, Karnovsky MJ (1980) Evaluation of the polyene antibiotic filipin as a cytochemical probe for membrane cholesterol. *J Histochem Cytochem* 28: 161–168

37. Shah AD, Inder KL, Shah AK, Cristino AS, McKie AB, Gabra H, Davis MJ, Hill MM (2016) Integrative analysis of subcellular quantitative proteomics studies reveals functional cytoskeleton membrane-lipid raft interactions in cancer. *J Proteome Res* 15: 3451-3462

38. Holland SJ, Pan A, Franci C, Hu Y, Chang B, Li W, Duan M, Torneros A, Yu J, Heckrodt TJ *et al* (2010) R428, a selective small molecule inhibitor of Axl kinase, blocks tumor spread and prolongs survival in models of metastatic breast cancer. *Cancer Res* 70: 1544–1554

39. Rea K, Pinciroli P, Sensi M, Alciato F, Bisaro B, Lozneanu L, Raspagliesi F, Centritto F, Cabodi S, Defilippi P *et al* (2015) Novel Axl-driven signaling pathway and molecular signature characterize high-grade ovarian cancer patients with poor clinical outcome. *Oncotarget* 6: 30859–30875

40. Huang RY, Antony J, Tan TZ, Tan DS (2017) Targeting the AXL signaling pathway in ovarian cancer. *Mol Cell Oncol* 4: e1263716

41. Lee HJ, Jeng YM, Chen YL, Chung L, Yuan RH (2014) Gas6/Axl pathway promotes tumor invasion through the transcriptional activation of Slug in hepatocellular carcinoma. *Carcinogenesis* 35: 769−775

42. Simons K, Ikonen E (1997) Functional rafts in cell membranes. *Nature* 387: 569−572

43. Ozhan G, Sezgin E, Wehner D, Pfister AS, Kuhl SJ, Kagermeier-Schenk B, Kuhl M, Schwille P, Weidinger G (2013) Lypd6 enhances Wnt/beta-catenin signaling by promoting Lrp6 phosphorylation in raft plasma membrane domains. *Dev Cell* 26: 331−345

44. Chen CL, Chen CY, Chen YP, Huang YB, Lin MW, Wu DC, Huang HT, Liu MY, Chang HW, Kao YC *et al* (2016) Betulinic acid enhances TGF-beta signaling by altering TGF-beta receptors partitioning between lipid-raft/caveolae and non-caveolae membrane microdomains in mink lung epithelial cells. *J Biomed Sci* 23: 30

45. Simons K, Toomre D (2000) Lipid rafts and signal transduction. *Nat Rev Mol Cell Biol* 1: 31−39

46. Della Peruta M, Martinelli G, Moratti E, Pintani D, Vezzalini M, Mafficini A, Grafone T, Iacobucci I, Soverini S, Murineddu M *et al* (2010) Protein tyrosine phosphatase receptor type gamma is a functional tumor suppressor gene specifically downregulated in chronic myeloid leukemia. *Cancer Res* 70: 8896−8906

47. Laczmanska I, Sasiadek MM (2011) Tyrosine phosphatases as a super-family of tumor suppressors in colorectal cancer. *Acta Biochim Pol* 58: 467−470

48. Cheung AK, Lung HL, Hung SC, Law EW, Cheng Y, Yau WL, Bangarusamy DK, Miller LD, Liu ET, Shao JY *et al* (2008) Functional analysis of a cell cycle-associated, tumor-suppressive gene, protein tyrosine phosphatase receptor type G, in nasopharyngeal carcinoma. *Cancer Res* 68: 8137−8145

49. Shu ST, Sugimoto Y, Liu S, Chang HL, Ye W, Wang LS, Huang YW, Yan P, Lin YC (2010) Function and regulatory mechanisms of the candidate tumor suppressor receptor protein tyrosine phosphatase gamma (PTPRG) in breast cancer cells. *Anticancer Res* 30: 1937−1946

50. Cheung AK, Ip JC, Chu AC, Cheng Y, Leong MM, Ko JM, Shuen WH, Lung HL, Lung ML (2015) PTPRG suppresses tumor growth and invasion via inhibition of Akt signaling in nasopharyngeal carcinoma. *Oncotarget* 6: 13434−13447

51. Mirenda M, Toffali L, Montresor A, Scardoni G, Sorio C, Laudanna C (2015) Protein tyrosine phosphatase receptor type gamma is a JAK phosphatase and negatively regulates leukocyte integrin activation. *J Immunol* 194: 2168−2179

52. Zanini E, Louis LS, Antony J, Karali E, Okon IS, McKie AB, Vaughan S, El-Bahrawy M, Stebbing J, Recchi C *et al* (2017) The tumor-suppressor protein OPCML potentiates anti-EGFR- and anti-HER2-targeted therapy in HER2-positive ovarian and breast cancer. *Mol Cancer Ther* 16: 2246−2256

53. Giles KM, Kalinowski FC, Candy PA, Epis MR, Zhang PM, Redfern AD, Stuart LM, Goodall GJ, Leedman PJ (2013) Axl mediates acquired resistance of head and neck cancer cells to the epidermal growth factor receptor inhibitor erlotinib. *Mol Cancer Ther* 12: 2541−2558

54. Zhang Z, Lee JC, Lin L, Olivas V, Au V, LaFramboise T, Abdel-Rahman M, Wang X, Levine AD, Rho JK *et al* (2012) Activation of the AXL kinase causes resistance to EGFR-targeted therapy in lung cancer. *Nat Genet* 44: 852−860

55. Langdon SP, Lawrie SS (2001) Establishment of ovarian cancer cell lines. *Methods Mol Med* 39: 155−159

56. Karpova T, McNally JG (2006) Detecting protein-protein interactions with CFP-YFP FRET by acceptor photobleaching. *Curr Protoc Cytom* Chapter 12: Unit12 17

57. Meder D, Moreno MJ, Verkade P, Vaz WL, Simons K (2006) Phase coexistence and connectivity in the apical membrane of polarized epithelial cells. *Proc Natl Acad Sci USA* 103: 329−334

58. Tibes R, Qiu Y, Lu Y, Hennessy B, Andreeff M, Mills GB, Kornblau SM (2006) Reverse phase protein array: validation of a novel proteomic technology and utility for analysis of primary leukemia specimens and hematopoietic stem cells. *Mol Cancer Ther* 5: 2512−2521

59. Sys G, Van Bockstal M, Forsyth R, Balke M, Poffyn B, Uyttendaele D, Bracke M, De Wever O (2012) Tumor grafts derived from sarcoma patients retain tumor morphology, viability, and invasion potential and indicate disease outcomes in the chick chorioallantoic membrane model. *Cancer Lett* 326: 69−78